CHALMERS
UNIVERSITY OF TECHNOLOGY

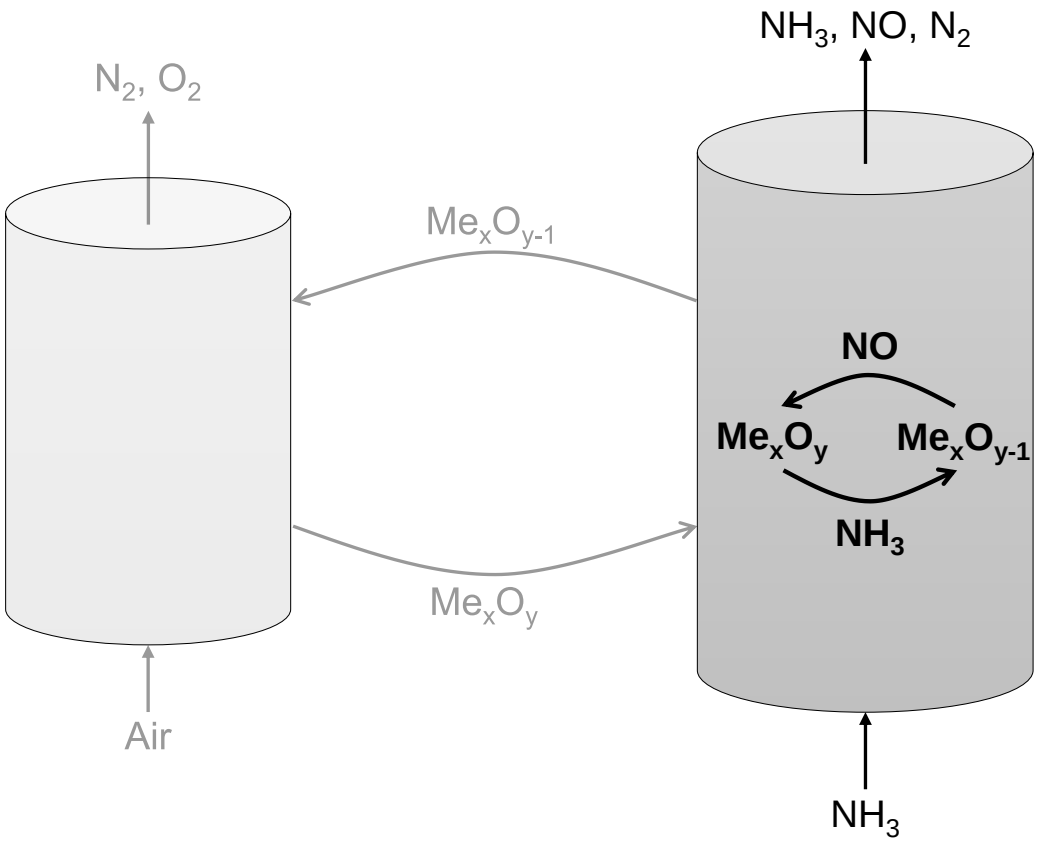

Fate of Fuel Nitrogen in Chemical Looping Combustion

Influence of Homogeneous and Heterogeneous Reactions

Master's thesis in Sustainable Energy Systems

ELLEN AUGUSTSSON

Department of Space, Earth and Environment
CHALMERS UNIVERSITY OF TECHNOLOGY
Gothenburg, Sweden 2019

Master's thesis 2019

Fate of Fuel Nitrogen in Chemical Looping Combustion

Influence of Homogeneous and Heterogeneous Reactions

ELLEN AUGUSTSSON

CHALMERS
UNIVERSITY OF TECHNOLOGY

Department of Space, Earth and Environment
Division of Energy Technology
Chalmers University of Technology
Gothenburg, Sweden 2019

Fate of Fuel Nitrogen in Chemical Looping Combustion
Influence of Homogeneous and Heterogeneous Reactions
ELLEN AUGUSTSSON

Supervisor: Tobias Mattisson, Department of Space, Earth and Environment
Examiner: Fredrik Normann, Department of Space, Earth and Environment

Master's Thesis 2019
Department of Space, Earth and Environment
Division of Energy Technology
Chalmers University of Technology
SE-412 96 Gothenburg
Telephone +46 31 772 1000

Cover: An illustration of a chemical looping combustion process with focus on the heterogeneous reactions involving nitrogen species.

Typeset in LaTeX
Printed by Chalmers Digitaltryck
Gothenburg, Sweden 2019

Fate of Fuel Nitrogen in Chemical Looping Combustion
Influence of Homogeneous and Heterogeneous Reactions
ELLEN AUGUSTSSON
Department of Space, Earth and Environment
Chalmers University of Technology

Abstract

Chemical looping combustion is a novel combustion technology that can be used to reduce CO_2 emissions. However, with nitrogen containing fuels, NO_x is expected to form. The mechanism of NO_x formation and reduction due to fuel bound nitrogen in chemical looping combustion is not well established. As a step in understanding this mechanism, this thesis aims to investigate the influence of homogeneous, gas-phase, reactions and heterogeneous, gas-solid, reactions causing NO_x formation and reduction in chemical looping combustion. This was done by combining modelling and experimental endeavours. Gas-phase modelling of important homogeneous reactions was performed using CHEMKIN. Furthermore, experiments were carried out with thermal gravimetric analysis to study the important heterogeneous reactions, for which kinetics were derived. Activated, Norwegian ilmenite was used as oxygen carrier, as this is currently a bench-mark oxygen carrier. The proposed reaction pathway that the modelling work and the experiments are based on suggests that the NO_x precursor NH_3 can be catalytically decomposed to N_2 or oxidised to NO by the oxygen carrier and that the formed NO can be reduced to N_2, either by the catalytic reaction with NH_3 or by oxidation of the reduced OC. The results indicated that the heterogeneous reactions are of large importance and that the environment in chemical looping combustion cannot be modelled using only gas-phase chemistry. The main conclusions are that the heterogeneous reactions seem to dominate the NO_x formation and reduction pathways and that NO_x formation is larger than NO_x reduction with respect to the heterogeneous reactions when utilising ilmenite as oxygen carrier.

Keywords: NO_x formation; NO_x reduction; Chemical looping combustion; Kinetics; Ilmenite; TGA

Acknowledgements

This thesis work was carried out under the framework of two projects financed by the National Science Foundation (VR): Project 2016-05487 and 2015-04371.

I would like to express my largest gratitude towards my examiner Fredrik Normann and my supervisor Tobias Mattisson for making this thesis possible and for their invaluable guidance and support throughout the thesis. Many thanks to Rikard Edland for teaching me CHEMKIN, for his essential advice related to the modelling work and for all helpful discussions. My deepest appreciation to Fredrik Hildor and Duygu Yilmaz for their invaluable guidance with the experimental part of this thesis, and for making the long days in the lab enjoyable. Thanks should also go to Burçak Ebin for instructing me on how to operate the TGA device.

I would like to express my gratitude towards the members of the OC group at Chalmers University of Technology for the interesting lunch seminars and discussions. Also, thanks to the colleagues at the division of Energy Technology for providing a pleasant working environment throughout my year as a thesis worker. An extra thanks to Ana and Irene, who made the autumn a little less grey, and to Julia and Linnéa, who made the spring a little sunnier.

I cannot leave Chalmers University of Technology without expressing my appreciation for Angelica Gyllén, who has inspired me since the first time I met her. Thank you for all the encouragement, support and pep talks.

Last but not least, to all of my near and dear ones who always support me and believe in me, thank you. A special thank you to Philip, I could not have done this without your support.

Ellen Augustsson, Gothenburg, June 2019

Contents

List of Figures

List of Tables

Nomenclature

Abbreviations

BECCS	Bio-Energy with Carbon Capture and Storage
CCS	Carbon Capture and Storage
CLC	Chemical Looping Combustion
CDLC	Coal Direct Looping Combustion
CLOU	Chemical Looping Oxygen Uncoupling
FB	Fluidised Bed
FBC	Fluidised Bed Combustion
GHG	Greenhouse Gas
OC	Oxygen Carrier
OCAC	Oxygen Carrier Aided Combustion
PFR	Plug Flow Reactor
Redox	Reduction and Oxidation
TGA	Thermal Gravimetric Analysis
XRD	X-Ray Diffraction

Greek Letters

β	Constant in the Modified Arrhenius Equation	-
ρ	Density	kg m^{-3}
τ	Time for Complete Solid Conversion	s
ω	Mass-Based Oxygen Carrier Conversion	-

Latin Letters

b	Stoichiometric Factor	mol_{OC}/mol_{gas}
C	Concentration	mol m^{-3}
E_a	Activation Energy	cal mol^{-1}
k	Rate Constant	mol,m,s^1
k_0	Pre-Exponential Factor	mol,m,s^1
m	Mass	kg
n	Order of Reaction	-
r	Radius	m
r_i	Rate of Reaction i	mol $m^{-3}s^{-1}$
R	Gas Constant	cal $K^{-1}mol^{-1}$
R_o	Oxygen Transport Capacity	-
t	Time	s
T	Temperature	K
X	Solid Conversion Level	-

Subscripts

eq	Equilibrium
g	Grain
m	Molar
o	Oxidised
r	Reduced

[1] Depends on the order of reaction

1
Introduction

1.1 Background

Global warming is an urgent problem affecting the entire world. In the Paris Agreement from 2015, 195 countries agreed to the binding deal of keeping the global temperature increase well below 2 °C compared to pre-industrial levels [1]. In order to limit warming below this level, actions must be taken to decrease greenhouse gas (GHG) emissions. The GHG that contributes the most to the greenhouse effect is carbon dioxide (CO_2), for which the global level in the atmosphere has increased by approximately 42.5 % in 2014 relative to pre-industrial levels [2]. Some of the main mitigation actions to reduce GHG emissions have been to reduce energy consumption, both by reducing the demand and by increasing the efficiency, as well as increasing the share of renewable energy sources [2]. However, more mitigation actions are needed as it is not believed that the current actions will be sufficient in order to meet the 2 °C limit [2].

Another approach to reduce the growing CO_2 emissions is to implement Carbon Capture and Storage (CCS) which purpose is to capture CO_2 emissions and store it in order to reduce the rate at which CO_2 is released into the atmosphere. The storage is for example done in saline aquifer formations or in ocean storage [3]. The conventional methods of carbon capture are however highly energy intense and require an increased fuel input to sustain the increased energy requirement [4]. Chemical looping combustion (CLC) is a technology that could be used as a capturing technology without a large energy penalty [5]. In CLC, an oxygen carrier (OC) is cycled between two reactors, one containing air and one containing fuel. The OC is oxidised in the air reactor, whereas it is reduced in the fuel reactor, allowing the fuel to be oxidised by the lattice oxygen found in the OC. In this manner, the flue gas from the fuel reactor consists mainly of CO_2 and water, where the latter easily can be condensed, creating a pure CO_2 stream ready for storage. To achieve "negative" CO_2 emissions, CCS would preferably be conducted in combination with carbon-neutral fuels, such as biomass [5]. This is called Bio-Energy with Carbon Capture and Storage (BECCS). With biomass, there is a zero net transfer of carbon during combustion due to the absorption of CO_2 through photosynthesis prior to combustion [6]. However, if the produced CO_2 instead is stored, there is an overall removal from the atmosphere [7].

Depending on the fuel used, the composition of the flue gases from the fuel reac-

tor will differ. In case of combustion of nitrogen containing fuels, nitrogen oxides (NO_x), i.e. NO, NO_2 and N_2O, will arise [8]. NO_x cause acid rain and photochemical smog [8] and N_2O is also a GHG which has a CO_2 equivalence of 298 [9]. Due to the absence of N_2 and the low combustion temperatures in CLC, NO_x can only form from fuel bound nitrogen [10]. The amount of NO_x emissions is greatly affected by the combustion environment and the initial concentration of fuel bound nitrogen [11]. The type of fuel bound nitrogen species is, however, of less importance with respect to the amount of NO_x emissions [11]. NO_x formation has been studied extensively in conventional combustion processes, i.e. in the presence of molecular oxygen. In most of those processes, the nitrogen chemistry is controlled by the gas-phase chemistry and the formation of radicals. However, in fluidised bed combustion (FBC), the presence and high flux of solid bed material make heterogeneous reactions important to consider [12]. In similarity to conventional FBC, CLC is usually utilising interconnected fluidised beds (FB), with the different being that the inert bed material is replaced with OC particles.

As of today, not many studies have investigated the mechanisms of NO_x formation in CLC. NO_x formation has been investigated experimentally, both for continuous CLC operation [5, 10, 13–19] and for batch experiments [14, 20–25] with varying results with respect to NO_x formation. Little work has been made to investigate the NO_x formation paths, and no kinetic evaluation has been conducted to the best of the author's knowledge.

1.2 Aim

This project aims to investigate which kinetic mechanisms that control the fuel bound nitrogen reaction paths in the fuel reactor in CLC. The influence of both homogeneous, gaseous, reactions and heterogeneous reactions between the gaseous compounds and the OC are investigated. The homogeneous reactions are evaluated based on whether the environment in CLC can be modelled using gas-phase chemistry to mimic the oxidation potential of the OC. To evaluate the heterogeneous reactions, experiments are conducted followed by a kinetic derivation.

1.3 Outline of This Thesis

In the following chapter, theoretical background is given regarding CLC, the reaction pathways for NO_x, both in general and what is expected in CLC, how nitrogen chemistry has been modelled in other heterogeneous systems and basics of kinetics. In Chapter 3, the results from the literature review of NO_x formation in CLC applications are presented. The method of this thesis, including both modelling and experimental approaches, is found in Chapter 4 followed by the results and discussion in Chapter 5 and 6 respectively. Finally, the conclusions are presented in Chapter 7.

2
Theory

In this chapter, information regarding aspects needed to consider in CLC is given. Information about NO_x and the general formation paths, as well as the formation paths relevant to CLC are presented. Also, a short overview of modelling approaches related to modelling of NO_x formation and reduction in heterogeneous systems is presented. Furthermore, the basics of kinetics is explained followed by kinetic models of gas-solid reactions relevant in CLC.

2.1 Carbon Capture and Storage - CCS

A method of decreasing the levels of CO_2 in the atmosphere and CO_2 emissions is to implement the technology CCS. The concept is to capture the produced CO_2 and thereafter store it in a manner that will not result in a rapid release of CO_2 to the atmosphere. To capture CO_2, three main subgroups exist; pre-combustion, post-combustion and oxyfuel-combustion [26]. In pre-combustion capture, the fuel is gasified to create a synthesis gas from which CO is reacted to CO_2 by addition of steam [26]. The CO_2 can thereafter be separated before the remaining H_2 is used for combustion. In post-combustion capture, the CO_2 is removed after combustion, which can be seen as a further step in the flue gas cleaning process [26]. Oxyfuel-combustion utilises pure oxygen as an oxidant instead of air, resulting in flue gas consisting of CO_2 and water [26], where the CO_2 can easily be separated by condensing the steam. All technologies account for a high energy penalty due to energy consuming gas separations [4]. Regarding the storage of the CO_2, there are various options, e.g. storage in deep saline formations and storage in oil and gas reservoirs [3].

2.2 Chemical Looping Combustion - CLC

CLC is a novel combustion technology which can be used with the purpose of CO_2 capture without the large energy penalty related to conventional capturing methods [2]. It consists of two interconnected fluidised bed reactors, one air reactor and one fuel reactor, where the OC is cycled between the reactors [27]. The schematic over a CLC-unit is presented in Figure 2.1.

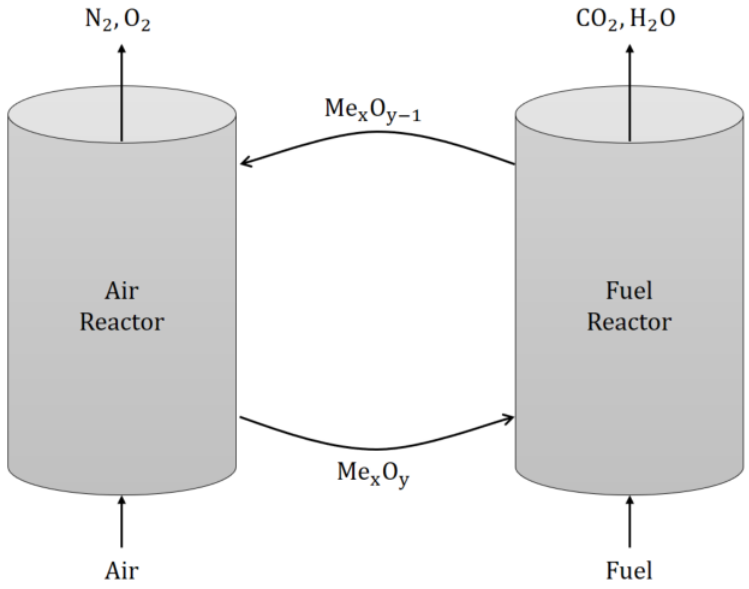

Figure 2.1: Schematics over a CLC-unit.

In the air reactor, the OC will be oxidised and the oxidation of a generic OC with the oxygen provided from air is presented below:

$$2\,\mathrm{Me}_x\mathrm{O}_{y-1} + \mathrm{O}_2 \longrightarrow 2\,\mathrm{Me}_x\mathrm{O}_y. \tag{2.1}$$

The gas stream out of the air reactor consists of N_2 and the excess oxygen not needed to oxidise the OC. The reaction in the air reactor (Equation (2.1)) is always exothermic [27].

In the fuel reactor, the OC will be reduced by the fuel. The reduction can occur to different reduction levels, i.e. not all OC needs to be in the same reduction state. Depending on the fuel used, different reactions will happen, and the following two equations describe the reduction of a generic OC with hydrogen (H_2) and carbon monoxide (CO):

$$\mathrm{Me}_x\mathrm{O}_y + \mathrm{CO} \longrightarrow \mathrm{Me}_x\mathrm{O}_{y-1} + \mathrm{CO}_2 \tag{2.2}$$

and

$$\mathrm{Me}_x\mathrm{O}_y + \mathrm{H}_2 \longrightarrow \mathrm{Me}_x\mathrm{O}_{y-1} + \mathrm{H}_2\mathrm{O}. \tag{2.3}$$

After the reduction, the reduced OC is returned to the air reactor and again oxidised with air. The flue gases from the fuel reactor consist of mainly CO_2 and water, where the steam can easily be condensed to create a CO_2-rich stream. The reactions in the fuel reactor can be either endothermic or exothermic, depending on the combination of OC and fuel [28]. The net energy release in the CLC-unit is the same as if the fuel would be conventionally combusted [17].

2.3 Chemical Looping Oxygen Uncoupling - CLOU

A process very similar to CLC is Chemical Looping Oxygen Uncoupling (CLOU). The schematics over a CLOU-process is the same as in CLC with the difference of that the OC undergoes thermal decomposition which releases molecular oxygen to the gas phase [29] instead of being reduced by the fuel. Thus, the reduction of the OC in CLOU can be expressed as:

$$2\,\mathrm{Me}_x\mathrm{O}_y \longrightarrow 2\,\mathrm{Me}_x\mathrm{O}_{y-1} + \mathrm{O}_2, \tag{2.4}$$

whereas the oxidation of the OC follows the same reaction characteristics as in normal CLC, i.e. as described in Equation (2.1). Due to the presence of molecular oxygen, the fuel in a CLOU-process is combusted as in conventional combustion, with the advantage of being in a nitrogen-free environment. For H_2 and CO (syngas), that is:

$$\mathrm{H}_2 + \mathrm{CO} + \mathrm{O}_2 \longrightarrow \mathrm{H}_2\mathrm{O} + \mathrm{CO}_2. \tag{2.5}$$

Suitable OC for CLOU purposes are metal oxides based on copper, manganese or cobalt, as these have suitable thermodynamic properties at relevant temperatures [4].

One advantage of using an OC with CLOU properties is the increased combustion rates with solid fuels compared to using a material lacking CLOU properties. When using solid fuels in normal CLC, the char is commonly gasified in the fuel reactor before combustion due to difficulties of the solid-solid reaction between the solid fuel particles and the lattice oxygen in the OC. In CLOU, where molecular oxygen is found freely in the gas phase, solid fuel particle can be combusted directly. The char gasification step is slow and if gasification can be avoided, the rate of the combustion process increases [30].

2.4 Oxygen Carrier - OC

The choice of OC is a crucial factor in CLC as it highly affects the operational performance. Different OC are suitable for different fuels, for example, an OC with CLOU properties could be favourable with solid fuels, see section 2.3 for further elaboration. Here follows a list of desired characteristics for OC in CLC applications, considering that they are used in FB systems [2, 4]. The OC should

(i) be environmentally non-hazardous
(ii) be able to transport enough oxygen for combustion, i.e. have sufficient oxygen capacity
(iii) have high reactivity during both reduction and oxidation
(iv) have a high fuel conversion towards CO_2 and H_2O with respect to thermodynamics
(v) have a high cyclic stability
(vi) not agglomerate or fragment easily

(vii) be cost effective

Nearly a thousand of OC materials have been experimentally investigated [2], with the transition metal oxides shown to have favourable properties [27]. The OC with most operating hours in CLC by the year 2016 are nickel-, copper- and iron-based OC [2]. However, the reaction rate often decreases rapidly with only a few reduction-oxidation (redox) cycles when using pure metal oxides, which favours the use of a support material [2]. The presence of a support material increases the mechanical strength as well as inhibits attrition of the OC [4], resulting in an improved cyclic stability.

The oxygen transport capacity is a measure of how much oxygen that can be theoretically stored in the OC and, thus, also be released in the CLC-unit. It can be expressed according to [31]:

$$R_o = \frac{m_o - m_r}{m_o}, \tag{2.6}$$

where R_o is defined as the oxygen transport capacity, m is the mass of the OC and the subscripts o and r refer to a level of full oxidation and full reduction respectively. For hematite (Fe_2O_3), copper oxide (CuO) and nickel oxide (NiO), the oxygen transport capacity is 0.03, 0.07 and 0.21 respectively [32]. The corresponding number for ilmenite, an OC based on Fe-Ti and the focus of this work, is 0.039 [13].

Furthermore, a way of classifying the oxidation level of an OC is by the mass-based OC conversion, ω. It is defined as [32]:

$$\omega_i = \frac{m_i}{m_o}, \tag{2.7}$$

where m_i is the mass of the OC at time i. At lower ω, the OC has lower potential of oxidising the fuel, as less oxygen is present in the material. A ω of one would correspond to an OC in its most oxidised state.

The solid conversion, X, can also be based on the active amount of oxygen in the material. During reduction and oxidation of the OC, the solid conversion on this basis can be expressed as [33]:

$$X_r = \frac{m_o - m}{R_o m_o} \tag{2.8}$$

and

$$X_o = \frac{m - m_r}{R_o m_o}. \tag{2.9}$$

2.4.1 Ilmenite

The focus of this work is on the OC ilmenite. Ilmenite has been subject of investigations in many studies related to CLC using various types of fuels [4], with

the result of ilmenite having good capability of being an OC in CLC. Ilmenite has been shown to possess great potential of oxidising syngas, with higher conversion of H_2 than CO [34, 35]. However, the conversion of CH_4 has been shown to be at moderate levels [34]. Ilmenite is a low-cost natural iron titanium ore, which in its reduced state consists mainly of $FeTiO_3$ ($FeO \cdot TiO_2$), where the active phase is the iron oxide [4]. Ilmenite can be oxidised to the final oxidation level according to:

$$4\,FeTiO_3 + O_2 \rightleftharpoons 2\,Fe_2TiO_5 + 2\,TiO_2. \tag{2.10}$$

It is also expected that ilmenite has the intermediate oxidation levels Fe_2O_3 and $Fe_2O_3 \cdot 2\,TiO_2$ [34].

Furthermore, replacing parts of the sand with ilmenite as bed material in FBC, in so called Oxygen Carrier Aided Combustion (OCAC), has been shown to have a favourable impact on the combustion system [36, 37]. It is believed that ilmenite contributes to an evener distribution of oxygen in the furnace, resulting in less combustible species at the outlet [37]. An added advantage is that oxygen can be stored in the furnace, thus moderating for variations in fuel flow and enabling the use of lower air-to-fuel ratios [38].

2.5 Nitrogen Oxides - NO_x

Nitrogen oxides (NO_x) is a term used to describe a various nitrogen containing compounds, most often referred to nitric oxide (NO), nitrogen dioxide (NO_2) and nitrous oxide (N_2O). The anthropogenic NO_x emissions are substantially larger than the endogenic. Among the anthropogenic emissions, the transport sector and coal-fired power plants are accountable for the majority. NO is the main NO_x product formed during combustion, whereas the equilibrium between NO and NO_2 is highly shifted towards NO_2 at atmospheric conditions. When NO_2 comes in contact with water, nitric acid (HNO_3) is formed, which is causing acid rain. NO_x emissions are also a precursor of photochemical smog by the production of tropospheric ozone. Moreover, NO_x emission is a cause of the depletion of the stratospheric ozone. N_2O is an analgesic [8] with a GHG-potential 298 times greater than that of CO_2 [9]. N_2O emissions have been found to be of importance in FBC, but of minor importance in other combustion systems [39].

In combustion processes, there are three distinct paths of NO_x formation; thermal NO_x, prompt NO_x and fuel NO_x which are described below.

2.5.1 Thermal NO_x

Thermal NO_x is created when molecular oxygen and molecular nitrogen react at high temperatures [39]. The extended Zeldovich mechanism describes this with the following reactions [39]:

$$N_2 + O \rightleftharpoons NO + N, \tag{2.11}$$

$$N + O_2 \rightleftharpoons NO + O, \tag{2.12}$$

and

$$N + OH \rightleftharpoons NO + H. \tag{2.13}$$

A large amount of energy is required to activate the dissociation of molecular nitrogen and, thus, the formation of thermal NO_x is only significant at temperatures above 1500 °C [39]. In combustion with no fuel bound nitrogen, thermal NO_x is the reason for the clear majority of the produced NO_x emissions.

Due to the absence of molecular nitrogen and the low temperatures in the fuel reactor in CLC, no formation of thermal NO_x is expected to occur.

2.5.2 Prompt NO_x

In fuel rich environments, hydrocarbon radicals, such as C and CH, are formed which can react with molecular nitrogen to produce fixed nitrogen species [40]. Examples of these reactions are as follows [41]:

$$C + N_2 \longrightarrow CN + N \tag{2.14}$$

and

$$CH + N_2 \longrightarrow HCN + N. \tag{2.15}$$

NO_x is thereafter formed by oxidation of the fixed nitrogen species. This mechanism is referred to as prompt NO_x and was identified by Fenimore in 1972 [42]. Prompt NO_x is only contributing with a small fraction to the total NO_x emissions [42].

2.5.3 Fuel NO_x

Different fuels have different nitrogen content, organically bound nitrogen is found in almost all solid fuels to different extents [39]. For solid fuels, nitrogen is bound to the fuel structure and it can be released both from the char conversion as well as in the form of a volatile matter released during pyrolysis [39]. The temperature, the heating rate and the fuel structure affect how the nitrogen is divided between the volatile matter and the char [39]. The nitrogen species that are released with the volatiles are mainly hydrogen cyanide (HCN) and ammonia (NH_3) [43]. For high-rank fuels, such as coal, HCN is considered the main nitrogen species released during pyrolysis whereas for low-rank fuels, such as biomass, NH_3 stands for the majority of nitrogen species in the volatiles [44]. The distribution of the nitrogen species released during pyrolysis is dependent on, in addition to fuel type, heating rate, final temperature and residence time [43].

The intermediate nitrogen species formed during combustion (HCN, NH_3, etc.) can react both with oxygen species to create NO and with the produced NO to form

N_2 [45]. For NH_3, the general reaction path is oxidation of NH_3 to NH_i radicals ($i = 0, 1, 2$), which can be oxidised to NO or react with NO to form N_2. The reaction path for the oxidation of NH_3 according to Miller and Bowman is presented in Figure 2.2 [11].

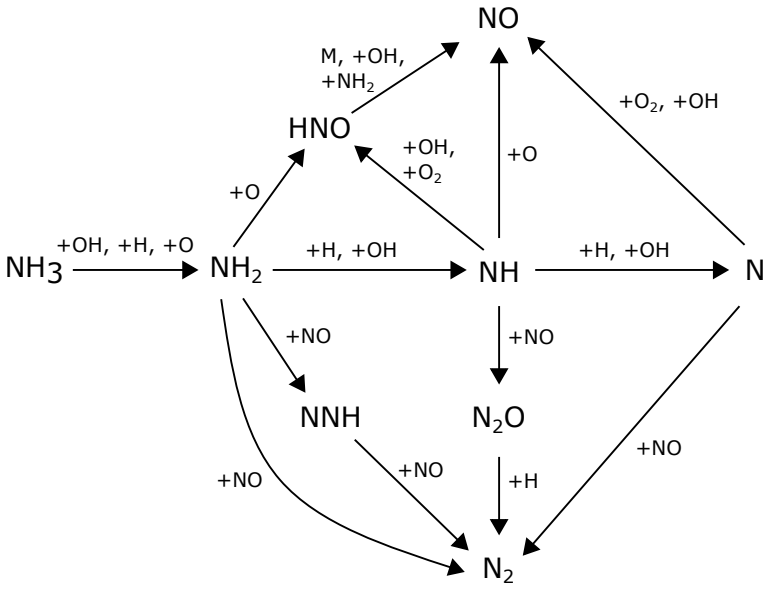

Figure 2.2: Reaction paths for the oxidation of NH_3 in combustion processes according to Miller and Bowman [11].

Furthermore, N_2 can also be formed without reacting with NO according to [11]:

$$NH_2 + NH \rightleftharpoons N_2H_2 + H, \tag{2.16}$$

$$N_2H_2 + M \rightleftharpoons NNH + H + M, \tag{2.17}$$

$$N_2H_2 + H \rightleftharpoons NNH + H_2, \tag{2.18}$$

and

$$NNH \rightleftharpoons N_2 + H. \tag{2.19}$$

However, for these reactions to occur, elemental nitrogen needs to be the dominating nitrogen species in the fuel [11]. This is most often not the case, which makes these reactions of minor importance to consider.

It is clear from the literature that when there is limited flux of solid materials, the radical chemistry is of high importance. However, in FBC as well as CLC, there is a significant solid concentration. Johnsson [43] investigated NO_x formation and reduction in FBC and concluded that it is unknown how the high solid concentration will affect the radical chemistry. Still, in subsequent models developed with respect to FBC and nitrogen chemistry, the heterogeneously catalysed reactions were dominating. Further, Löffler et al. [46] developed a mechanism describing NO_x formation

in FB, in which they proposed that the high solid concentration is causing radical quenching. The mechanism included the radical recombination reactions of O, H, OH, and HO_2 that occur on the surfaces of the solid bed material. Radical quenching is also included in the work of Kilpinen et at. [47], where NO_x formation and reduction are modelled in FBC.

2.6 Nitrogen Chemistry in CLC

There is very limited research around the nitrogen chemistry in the fuel reactor in CLC, characterised by mildly reducing atmosphere and the presence of OC. In relation to the research performed around nitrogen chemistry in normal combustion, the research is almost nonexistent. Most work around nitrogen chemistry in CLC has concentrated around the oxidation of NH_3 with OC. The use of NH_3 in these studies is motivated by the fact that NH_3 is less hazardous than HCN, which simplifies the experimental setup. Furthermore, in biomass, NH_3 is considered the dominating nitrogen species found in the volatiles [44]. Linderholm et al. [17], found that NH_3 is the main NO_x precursor found in a 100 kW pilot CLC plant when using bituminous coal. Jensen et al. [12] developed a model describing the formation and reduction of NO_x in pressurised FBC, with the simplification of assuming NH_3 as the sole nitrogen containing species found in the volatiles. The simplification was supported by laboratory experiments that showed that NH_3 and HCN exhibit similar selectivity towards NO when oxidised catalytically [12]. Similar behaviour could be expected when oxidising heterogeneously with OC, although it is important to consider that the OC can react non-catalytically in addition to catalytically. This section will focus on NH_3 as fuel bound nitrogen species, and, thus, this section will describe the possible reaction paths for NH_3 and the produced NO relevant in the fuel reactor in CLC. Note that all following reactions are overall reactions.

NH_3 can be oxidised by the OC, forming either NO or N_2 according to:

$$5\,\mathrm{Me}_x\mathrm{O}_y + 2\,\mathrm{NH}_3 \longrightarrow 5\,\mathrm{Me}_x\mathrm{O}_{y-1} + 2\,\mathrm{NO} + 3\,\mathrm{H}_2\mathrm{O} \tag{2.20}$$

and

$$3\,\mathrm{Me}_x\mathrm{O}_y + 2\,\mathrm{NH}_3 \longrightarrow 3\,\mathrm{Me}_x\mathrm{O}_{y-1} + \mathrm{N}_2 + 3\,\mathrm{H}_2\mathrm{O}. \tag{2.21}$$

The selectivity of the oxidation products is shown to be dependent on the type of OC [20], temperature [20] and oxidation level of the OC [25]. At temperatures relevant to CLC, NO is the dominating NO_x product.

Moreover, NO may be reduced by the reduced OC as follows:

$$2\,\mathrm{NO} + 2\,\mathrm{Me}_x\mathrm{O}_{y-1} \longrightarrow \mathrm{N}_2 + 2\,\mathrm{Me}_x\mathrm{O}_y. \tag{2.22}$$

Mayrhuber [22] found that reduced ilmenite could reduce NO with great success and Heezius [48] showed similar behaviour with magnetite ore.

Furthermore, it is believed that the OC could possess catalytic properties. The possible reactions that could be catalytically enhanced are:

$$2\,NH_3 \xrightarrow{Me_xO_y} N_2 + 3\,H_2, \tag{2.23}$$

$$6\,NO + 4\,NH_3 \xrightarrow{Me_xO_y} 5\,N_2 + 6\,H_2O, \tag{2.24}$$

and

$$NO + CO/H_2\,/C_xH_y \xrightarrow{Me_xO_y} N_2 + CO_2/H_2O. \tag{2.25}$$

The decomposition of NH_3 (Equation (2.23)) is catalytically enhanced by quartz sand [49]. Iron-based catalysts have been investigated with respect to the catalytic decomposition of NH_3, in which some catalytic activity have been detected, however to a small extent [50]. The presence of OC could also enhance the reduction of NO with NH_3 (Equation (2.24)). Both Cheng et al. [23] and Mayrhuber [22] investigated the effect of reduction of NO with syngas (Equation (2.25)) with the OC ilmenite. According to Cheng et al. [23], syngas does not seem to reduce NO. The presence of syngas is, however, reducing the OC, resulting in that the selectivity of the nitrogen containing species is increased toward N_2. Mayrhuber [22] also concluded that the presence of syngas is inhibiting the reduction of NO. However, in contrary to the findings of Cheng et al. [23], Mayrhuber [22] suggests that the NO formation from NH_3 is promoted by the presence of syngas.

2.7 Modelling of Nitrogen Chemistry

Due to the environmental effects of NO_x, the formation and the reduction of NO_x have been subject of investigation in various applications. Herein, examples of modelling of nitrogen chemistry in heterogeneous systems are presented.

A great amount of work has been done regarding modelling of NO_x formation and reduction in normal FBC, with different levels of details, both with respect to hydrodynamics and to nitrogen chemistry. Herein follows a short overview of the approaches used in modelling of NO_x formation and reduction in FBC, however, only with respect to nitrogen chemistry. It is believed that FBC conditions resemble those present in CLC in some way, i.e. significant loading of solid material and temperatures below 1000 °C. Still, the gas-phase atmosphere differs significantly, in addition to the absence of OC. The included reaction pathways for the modelling work are presented in Table 2.1. Zhao [51] developed a model where the main focus of the model comprised of NO_x arising from the fuel NO_x formation route (see Section 2.5.3) due to the relatively low combustion temperatures in FBC. Goel et al. [52] proposed a 15-step mechanism describing the heterogeneous reactions of coal combustion in FBC. NO is created by surface reactions initiated by the oxidation of the surface-bound species CN while N_2 is only formed by reduction of either NO or N_2O. For N_2 production in the former case, surface-bound NO is reduced by surface-bound CO while in the latter case, N_2O is reduced with C that is providing

a free site. Kilpinen et al. [47] included homogeneous gas-phase reactions, heterogeneous gas-solid reactions and heterogeneous catalytic reactions in their model. The mechanism for the gas-phase kinetics consists of approximately 300 elementary reactions and is including the effect of radical quenching due to high solid concentration.

Table 2.1: Included reaction pathways in the modelling work of NO_x formation and reduction in CFB combustion found in the literature.

	Zhao [51]	Goel et al. [52]	Kilpinen et al. [47]
Homogeneous reactions			
Extensive mechanism			X
Formation of NO	X		X[1]
Reduction of NO with NH_3 oxidation	X		X[1]
Heterogeneous reactions			
Formation of CO and CO_2		X	X
Formation of NO	X	X	X
Formation of N_2O		X	X
Reduction of NO	X	X	X
Reduction of N_2O		X	X
Catalytic reactions			
Reduction of N_2O			X
Formation of NO by NH_3 oxidation			X
Formation of N_2 by NH_3 oxidation			X
Reduction of NO with NH_3			X
Reduction of NO with CO	X		X
Decomposition of NH_3			X

[1] Included in "Extensive mechanism"

Both Jensen [53] and Edland [54] used similar kinetic models to describe NO_x forma-

tion and reduction in the presence of char, however in different applications. Jensen work was concentrated around cement production while Edland focused on iron ore pelletisation. To describe the formation and reduction of NO_x, they used gas-phase kinetics derived from Glarborg and Mendiara [55] (described in Section 4.2) with the addition of three heterogeneous reactions. The heterogeneous reactions describe char oxidation, NO formation from char-nitrogen and NO reduction by char.

Thengane et al. [56] investigated the oxidation of NH_3 with a metal oxide with the purpose of producing NO and H_2. They proposed that NH_3 would be absorbed on the surface of the metal oxide, enabling reactions between NH_3 and lattice oxygen found in the metal oxide. A gas-metal oxide would form in which intermediate nitrogen species would form to lastly be desorbed from the surface either as NO or N_2. Figure 2.3 shows the reaction mechanism described above with the metal oxide CuO. They concluded that the selectivity between NO and N_2 is controlled by the temperature and available lattice oxygen - high temperatures and high amounts of available lattice oxygen favours NO formation.

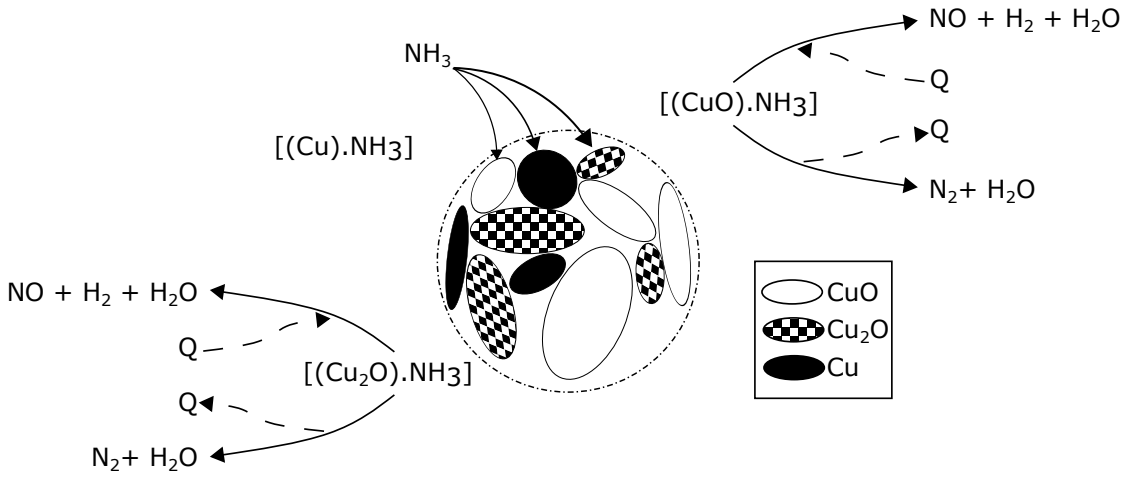

Figure 2.3: Reaction mechanism for the metal oxide CuO with NH_3, recreated from Thengane et al. [56].

2.8 Kinetics

In general, the rate of reaction is a function of temperature and the concentrations of the reactant species, expressed as follows [57]:

$$r_i = F\Big(T, \sum_J [J]\Big), \tag{2.26}$$

where r_i is the reaction rate with respect to species i, T is the temperature and $[J]$ is the concentration of species J. The unit of the reaction rate is normally mol/m^3s, but for reactions involving solids, both catalytic and non-catalytic reactions, the reaction rate may be expressed in terms of mass or moles of solid material.

For irreversible reactions, one simplification regarding Equation (2.26) is commonly implemented where the temperature dependency and the concentration dependency can be separated into two functions [57]:

$$r_i = \pm k(T) F\Big(\sum_J [J]\Big), \tag{2.27}$$

where k is denoted as the rate constant, which has a temperature dependency, and F is a function of the concentrations. Depending on whether species i refers to a product or a reactant, the sign will change since the rate of reaction either describes a production or a consumption of species.

A further simplification regarding the function describing the concentration dependency can be expressed as [57]:

$$F\Big(\sum_J [J]\Big) = \prod_J [J]^{\alpha_J}, \tag{2.28}$$

where α_J is the order of reaction with respect to species J.

The rate constant is often expressed using the Arrhenius relationship [57]:

$$k(T) = k_0 \cdot \exp(-E_a/RT), \tag{2.29}$$

where k_0 is a pre-exponential factor which does not have any temperature or concentration dependency, E_a is the activation energy for the reaction to occur and R is the gas constant. The unit of the rate constant depends on the overall order of reaction, i.e. it is adjusted in order to achieve the correct unit of the reaction rate. Furthermore, the Arrhenius equation can be modified into containing an explicit temperature dependency according to [58]:

$$k_{mod}(T) = k_0 T^{\beta} \exp(-E_a/RT), \tag{2.30}$$

where k_{mod} is the modified rate constant and β is a dimensionless parameter.

To obtain the constants in the Arrhenius relationship for a reaction, the logarithm of the rate constant expressed using Equation (2.29) can be utilised [57]:

$$\ln(k) = \ln(k_0) - \frac{E_a}{RT}. \tag{2.31}$$

Equation (2.31) has a linear dependency to $1/T$, where $\ln(k_0)$ and $-E_a/R$ correspond to the intercept with the y-axis and to the first derivative respectively. The plot of Equation (2.31), with $\ln(k)$ as y-variable and $1/T$ as x-variable is called an Arrhenius plot [57].

2.8.1 Kinetic Modelling of Gas-Solid Reactions

When modelling gas-solid reactions, different phenomena need to be considered, including external and internal mass transfer and kinetics [59].

In deriving redox kinetics for CLC, the shrinking core model, the changing grain size model and the nucleation model have previously been applied [60]. Most of the work has concentrated around the oxidation with oxygen and the reduction with ordinary gaseous fuels, such as CH_4 and syngas.

In the shrinking core model, the reaction starts at the surface of the core [61]. As the reaction proceeds, a product layer is produced around the core, resulting in that the reaction is occurring closer to the centre of the particle [61]. Thus, the product layer is increasing with time as the core size is decreasing. The core is considered nonporous whereas the product layer is considered porous [62]. The model takes into account (1) external mass transfer through the gas film, (2) internal mass transfer through the product layer and (3) the chemical reaction [27]. According to the shrinking core model, the change in the conversion level of the OC with time can be expressed as [59]:

$$\frac{dX}{dt} = \frac{3}{\tau}(1-X)^{2/3}. \tag{2.32}$$

Equation (2.32) is valid for a spherical geometry, but similar equations can be derived for other geometries. The time for complete solid conversion, τ, is expressed as [59]:

$$\tau = \frac{\rho_m r_g}{bk(C^n - C_{eq}^n)}, \tag{2.33}$$

where ρ_m is the molar density of OC in the solid, r_g is the grain radius, b is a stoichiometric factor, k is the rate constant based on the Arrhenius equation, C is the gas concentration, C_{eq} is the gas concentration at equilibrium and n is the reaction order. If the reverse reaction is negligible, the gas concentration at equilibrium can be set to zero.

3
Literature Review

NO_x formation in CLC-applications has been investigated experimentally previously. However, the formation paths with respect to kinetics have not been studied to the best of the author's knowledge. A great deal of the work that has been conducted in laboratory-scale FB reactors has been executed at Chalmers University of Technology in previous master's theses and research projects. Additionally, NO_x emissions in continuous CLC operation have been investigated in 0.5 kW - 100 kW CLC units with varying results on NO_x formation.

3.1 Batch Reactor Experiments

Herein, a summary of the previous work conducted in batch reactors related to nitrogen chemistry in CLC is presented. A short introduction to what has been studied is found in Table 3.1, followed by the conclusions of each work. A thorough overview of the results can be found in Table A.1 in Appendix A.

Table 3.1: Summary over the batch reactor experiments found in the literature.

Literature	**OC**	**Fuel**	**N-species**
Neumann [21]	CuO Calcinated ilmenite Activated ilmenite	No fuel Syngas	NH_3
Östergren [24]	Fe_2O_3 Ilmenite	Wood char	From solid fuel
Gu et al. [14]	Fe_2O_3	Bituminous coal Petcoke	From solid fuel
Cheng et al. [23]	Ilmenite	No fuel Syngas	NH_3
Wismer [20]	Fe_2O_3 Mn_3O_4	Syngas	NH_3
Normann et al. [25]	CuO	No fuel Syngas	NH_3
Mayrhuber [22]	Rock ilmenite Sand ilmenite	No fuel Syngas	NH_3 NO

Neumann [21] investigated the selectivity between N_2 and NO_x formation from NH_3 in different compositions of syngas and NH_3 diluted in N_2 in a laboratory-scale FB reactor. The experiments were conducted with activated ilmenite, calcinated ilmenite and copper oxide as OC. For calcinated ilmenite, the NO formation increased with increased temperature, while no explicit trend could be found for copper oxide. Copper oxide had a complete NH_3 conversion while for calcinated ilmenite, 6.4-0.2 % of residual NH_3 was found in the outlet for the temperature interval 850-950 °C. A high inlet fraction of NH_3 promoted higher NO formation, in terms of both actual numbers and in nitrogen selectivity, for all OC except activated ilmenite for which no trend was found. Furthermore, copper oxide had a higher fuel conversion of CO than ilmenite.

Östergren [24] studied the nitrogen products when using solid fuel, a Swedish wood chip, in a laboratory-scale FB reactor with the OC ilmenite and hematite. Steam was used as a gasification medium and the varied parameters were the steam fraction and temperature. Ilmenite showed a lower NO_x formation than hematite, while hematite showed a higher fuel conversion. An increased steam fraction reduced NO_x formation for ilmenite and the opposite for hematite. Furthermore, the type of OC seemed to impact NO_x formation more than the steam fraction did.

Gu et al. [14] performed solid fuel experiments, both in a laboratory-scale FB reactor and in a continuous 1 kW_{th} CLC prototype, with an iron ore as OC. In the batch experiments, petcoke and bituminous coal were used as fuels, whereas only the latter was used in the continuous setup. How various parameters, such as temperature and gasification medium, affected the NO_x release was investigated. For bituminous coal, the NO formation was promoted by the use of H_2O as gasification medium compared to CO_2 in the temperature range 850-950 °C, whereas for the temperature 1000 °C it was reversed. For petcoke, the NO formation was favoured by using the gasification medium H_2O over CO_2 at all studied temperatures.

Cheng et al. [23] investigated experimentally the possible reactions between NH_3 as nitrogen species and the OC ilmenite in a laboratory-scale FB reactor. In addition to NH_3, they used syngas as reducing gas. They concluded that the catalytic decomposition of NH_3 was an important reaction and that ilmenite showed a high conversion with respect to NH_3. Furthermore, they found that the temperature (in the investigated temperature range 850-950 °C) was only of minor importance regarding the nitrogen selectivity. However, the nitrogen selectivity was shown to be highly affected by the inlet concentrations of both NH_3 and syngas. They also concluded that reduced ilmenite showed a great potential of reducing NO to N_2.

Wismer [20] studied the behaviour of three OC, a Fe-, a Mn- and a Ni-based, in a laboratory-scale FB reactor with the reducing gases consisting of NH_3 and syngas in different volume fractions. The conclusion of this study was that the Ni-based OC was preferable with respect to NO emissions as no NO was found in that case. However, this kind of OC is expensive and is not suitable for operation with sulphur containing fuel as it deactivates the OC. The Mn-based OC showed a high

fuel conversion with respect to CO but also high NO formation. The third OC, the Fe-based, resulted in a low fuel conversion but a high NO formation. Regarding the oxidation potential of the OC, it was concluded that it should be high enough to combust the fuel but low enough to suppress the oxidation of NH_3.

Normann et al. [25] investigated the effect of using an OC with CLOU properties, copper oxide, with respect to the oxidation of NH_3. The experiments were conducted in a laboratory-scale FB reactor with syngas as fuel and the inlet fractions of NH_3 and syngas were altered respectively. They concluded that the nitrogen selectivity was highly dependent on the oxidation level of the OC; a higher oxidation level promoted the nitrogen selectivity towards NO. They also found that the nitrogen selectivity was affected by syngas, a higher concentration of syngas seemed to hinder NO formation. The ageing of the OC was also investigated with the result of decreasing the nitrogen selectivity to NO.

Mayrhuber [22] performed pulse experiments in a laboratory-scale FB reactor with two kinds of ilmenite; a rock ilmenite from Norway and a sand ilmenite from Australia. Mayrhuber used both NH_3 and NO as introduced nitrogen species and syngas as fuel. The result of this project was that the NO formation decreased with increased temperature and that the mass-based OC conversion, ω, needed to be above 0.99 to achieve NO formation. Furthermore, the reduction reaction between NO and the reduced OC seemed to be of importance whereas the outlet NO concentration was not affected by what nitrogen species that was introduced to the reactor. The two ilmenites showed different behaviours regarding nitrogen selectivity and also regarding NH_3 conversion, as the rock ilmenite succeeded to fully oxidise NH_3 and with the sand ilmenite, up to 5 % of residual NH_3 was found.

With respect to the studies above, it is important to consider the reactor units used. Almost all experimental data was retrieved from FB units. It is well known that this type of arrangement can have a significant bypass of gas in bubbles, meaning that the actual concentration of gas that the particles are exposed to is not well known.

3.2 Continuous CLC Operation

First, a short overview concerning nitrogen chemistry in continuous CLC operation is presented in Table 3.2, thereafter, the findings of each study is discussed. For a thorough summary regarding the results, see Table A.2 in Appendix A.

Table 3.2: Summary over the continuous CLC operation found in the literature.

Literature	**Size (kW)**	**OC**	**Fuel**
Linderholm et al. [15]	100	Ilmenite	Swedish wood char Mexican petroleum coke
Mendiara et al. [10]	0.5	Ilmenite	Spanish lignite
Gu et al. [14]	1	Fe_2O_3	Bituminous coal
Song et al. [16]	1	NiO	Shenhua bituminous coal Huaibei anthracite
Linderholm et al. [17]	100	Ilmenite	Bituminous coal
Bayham et al. [18]	25	Fe_2O_3	Sub-bituminous coal
Song et al. [19]	1	Fe_2O_3	Shenhua bituminous coal Huaibei anthracite
Markström et al. [13]	100	Ilmenite	Bituminous coal
Mendiara et al. [5]	0.5	Fe_2O_3	Pine sawdust Olive stone Almond shell

Linderholm et al. [15] investigated NO formation in a 100 kW CLC unit with solid fuels and the OC ilmenite. When using petcoke, they found that 3-8 % of the fuel nitrogen was converted to NO at 148 kW whilst a 20 % NO-conversion was obtained at 72 kW. They also found that the temperature affected the NO formation. Furthermore, NO formation was promoted by an increased circulation of the solid material.

Mendiara et al. [10] performed solid fuel experiments in a 500 W CLC-unit with lignite as fuel and ilmenite as OC. The result of their study was that the only NO_x compound found of significant magnitude was NO. However, 99 % of the fuel nitrogen was converted to N_2 in the fuel reactor. The air reactor gave rise to NO_x emissions by combustion of unconverted char, which are below the limits in the EU.

Gu et al. [14] examined the NO formation in a continuous 1 kW CLC prototype with bituminous coal and an iron ore as OC. They varied the temperature and the gasification medium. To achieve low NO formation, the process should be operated

at a high fuel reactor temperature and with H_2O as gasification medium. Moreover, they found that the major part of the NO_x emissions arose from the air reactor.

Song et al. [16] studied the conversion of fuel nitrogen in a 1 kW CLC prototype with different kinds of coal and a Ni-based OC. In the fuel reactor, all fuel nitrogen was converted to N_2 regardless of fuel type. In the air reactor, approximately 17-19 % of the char nitrogen was converted to NO and was promoted by an increased temperature.

Linderholm et al. [17] conducted continuous CLC experiments in a 100 kW unit with bituminous coal and ilmenite as OC. They found that 62 % of the fuel nitrogen was converted into gaseous compounds with the distribution being 1 wt-% HCN, 11 wt-% NO, 26 wt-% NH_3 and the remaining was assumed to be N_2.

Bayham et al. [18] investigated the behaviour of a 25 kW Coal Direct Chemical Looping (CDCL) unit with a Fe-based OC. CDCL is a similar process to CLC, where gasification enhancers are utilised. They found that 10-15 % of the fuel nitrogen was converted to NO_x in the fuel reactor, whereas no NO_x emissions were reported in the air reactor.

Song et al. [19] performed continuous operation of a 1 kW CLC unit with bituminous coal and anthracite. The OC used in the experiments was the iron ore hematite. The results of this study were that no NO was produced in the fuel reactor, whilst some NO was formed in the air reactor. The only product formed from the fuel nitrogen in the fuel reactor was N_2 and an increased temperature enhanced the fuel conversion to N_2. An increased temperature suppressed NO formation in the air reactor due to less unconverted char being transported into the air reactor at higher temperatures.

Markström et al. [13] conducted solid fuel operation of a 100 kW CLC unit with bituminous coal and ilmenite as an OC. Based on the maximum amount of NO that theoretically could be formed, they found that 10-20 % of the fuel nitrogen was converted to NO. Furthermore, a decreased flow in the fuel reactor resulted in a decrease in NO formation, whereas an increase of the flow in the air reactor resulted in an increase in NO formation.

Mendiara et al. [5] investigated the possibility of utilising CLC with biomass to achieve negative emissions by the technology BECCS. Three different kinds of biomass with different nitrogen contents were used with an iron ore as OC. They found a nitrogen conversion of 4-14 wt-% to NO with N_2 being the dominant nitrogen species in the outlet. By increasing the fuel reactor temperature, NO formation was reduced. No trend regarding NO formation was detected between the different biomasses.

3.3 Summary

To summarise the results from the batch reactor experiments, the type and oxidation state of the OC seem to be of great importance, both with respect to nitrogen conversion and fuel conversion. Even a specific material like ilmenite shows inconclusive results between batches - NH_3 conversion between 80 % and 100 % have been reported. Furthermore, the temperature dependency of NO_x formation with ilmenite is not established. Cheng et al. [23] reported that the selectivity between NO and N_2 was not affected by the temperature, Mayrhuber [22] reported lower NO formation at increased temperatures and Neumann [21] found an increased NO formation with increased temperatures. In general, for the investigated OC, an increase in concentration of the introduced nitrogen species results in higher NO_x formation with an exception of activated ilmenite where no trend could be seen according to Neumann [21]. The reasons for inconclusive results when using ilmenite compared to other OC could be that there exist different types of ilmenite with different properties depending on from where it is mined.

In continuous CLC operation, the general conclusion is that the main NO_x emissions arise from the air reactor due to unconverted char. However, not all studies distinguish between the emissions from the air reactor and the emissions from the fuel reactor. Bayham et al. [18] report NO_x emissions in the fuel reactor but no in the air reactor, however, they are using CDCL, which is not the same process as traditional CLC. The temperature dependency is not clear as Gu et al. [14], Song et al. [19] and Mendiara et al. [5] report a decrease in NO_x emissions with an increased temperature whereas Song et al. [16] found that the NO_x emissions are promoted by an increased temperature. Although, NO_x emissions from the fuel reactor may be of larger magnitude in future scenarios, as the fuel conversion is expected to increase.

The limited work and the, somewhat, conflicting results suggest that more research regarding NO_x formation in CLC is needed. This could also be of interest in other processes, for example in OCAC, where the need of further studies regarding NO_x formation has been expressed [38, 63].

4
Method

The method of this project is to apply the present understanding of nitrogen chemistry to conditions relevant to the fuel reactor in CLC and discuss it in relation to modelling and experimental findings. The gas-phase chemistry is modelled using a reaction mechanism including well established gas-phase reactions with the aim of investigating the possibility to model the environment in CLC using only gas-phase chemistry. The reaction mechanism is thereafter extended to also include heterogeneous reactions and catalysed reactions. To obtain kinetic parameters for this purpose, data from previous batch reactor experiments is used. In addition, experiments in a Thermal Gravimetric Analysis (TGA) are conducted for which kinetic parameters for the pure heterogeneous reactions are obtained, these are, however, not included in the modelling work.

4.1 Reaction Pathway Model

Herein follows a proposed reaction pathway for which the heterogeneous modelling and the experimental setup within this thesis is based upon. A similar approach as in the work of Jensen [53] and Edland [54] is used, where the fuel nitrogen is converted to NO and thereafter reduced to N_2. This reaction pathway is also proposed in some of the modelling of NO_x formation and reduction in FBC, for example in the work by Goel et al [52]. Furthermore, the reaction with hydrocarbons (Equation (2.25)) are not considered in this work. In terms of reactions, the heterogeneous reactions described in Equation (2.20) and Equation (2.22) and the catalytic homogeneous reactions described in Equation (2.23-2.24) are included in the proposed reaction pathway. The reaction pathway is presented in Figure 4.1, both with respect to the nitrogen species (Figure 4.1a) and to the OC (Figure 4.1b).

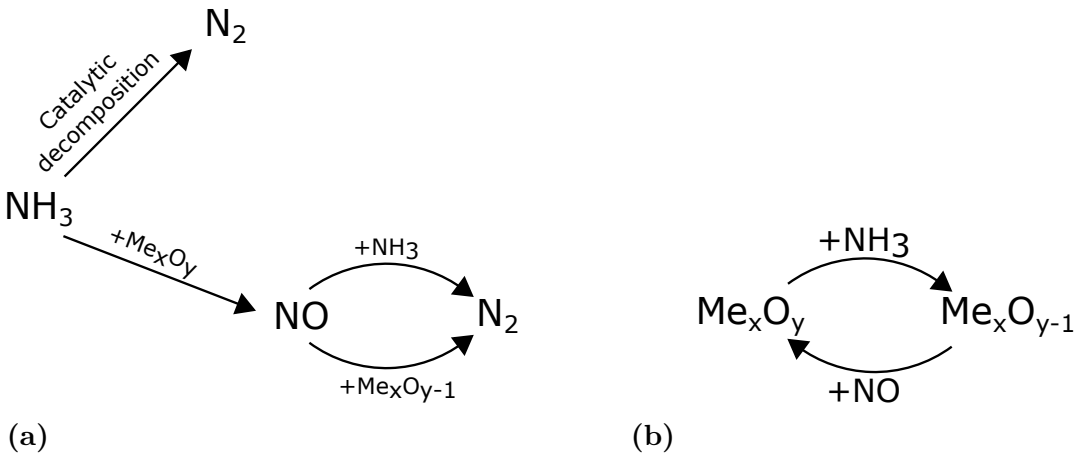

(a) **(b)**

Figure 4.1: Reaction pathway of nitrogen chemistry in CLC with respect to (a) the nitrogen species and (b) the OC.

4.2 Detailed Reaction Modelling

The modelling of the CLC-unit is performed in the software *CHEMKIN* using the extensive chemical kinetic model created by Mendiara and Glarborg [55]. The mechanism describes the homogeneous gas-phase reactions for nitrogen species and hydrocarbons in combustion applications. The model is restricted to hydrocarbons no larger than C_2 and is based on experimental work and thermodynamic data. The reaction mechanism consists of 779 elementary reactions with 97 species. The kinetics for the forward reactions is calculated with parameters from the modified Arrhenius equations, see Equation (2.30). For elementary reactions, the reaction is of first order with respect to each reactant.

To model the CLC-unit, a plug flow reactor (PFR) is used as reactor model. The dimensions and operating conditions are presented in Table 4.1. If nothing else is stated, the dimensions of the PFR correspond to the reactor used in most of the previous experimental work performed at Chalmers University of Technology. Most of the batch reactor experiments used a FB setup, where the gas may not necessarily move according to a plug flow. Still, it is a good approximation in describing the flow pattern. The reactor is operated isothermal and the temperature is altered in the interval 850-1150 °C in the simulations. Atmospheric pressure is used in all simulations and the temperatures and pressure are chosen to mimic the conditions in the fuel reactor in CLC.

Table 4.1: Dimensions and operating conditions for the modelled PFR.

Parameter	Value
d_i (mm)	22
z (mm)	870
P (atm)	1
T (°C)	850-1150
$\dot{V}_{inlet1}$ (cm^3/s)	15

4.2.1 Homogeneous Reactions

To investigate whether the environment in a CLC-unit can be modelled using only gas-phase chemistry, either CO/CO_2 or H_2/H_2O are used in varying inlet fractions. The purpose of varying the inlet fractions is to obtain different oxidation potentials as the gas is expected to be exposed to variable oxidation potentials in CLC. The simulations are performed both with and without the presence of a nitrogen species. In Table 4.2, an overview of these simulations is presented.

Table 4.2: Inlet conditions for the simulations investigating the environment in a CLC-unit using CO/CO_2 and H_2/H_2O to determine the reduction potential.

$\mathbf{x}_{CO}$	$\mathbf{x}_{CO_2}$	$\mathbf{x}_{H_2}$	$\mathbf{x}_{H_2O}$	$\mathbf{x}_{NH_3}$
0-0.990	1.000-0.100	-	-	-
0-0.895	0.990-0.095	-	-	0.010
-	-	0.010-0.900	0.990-0.100	-
-	-	0-0.895	0.990-0.095	0.010

To further resemble the environment in a CLC-unit, some combustion activity is introduced to the system. This is done by adding the combustion reactants syngas and oxygen in stoichiometric ratios. This could also be correlated to the use of CLOU materials, as oxygen is released to the gas phase. Furthermore, the availability of oxygen highly affects the radical chemistry - minor amounts could have a significant effect. To model this, two inlets are used; one which determines the reduction potential of the environment and one which contains the combustion reactants. All the CO/CO_2 or H_2/H_2O are added in the inlet of the reactor and are assumed to be well-mixed but move according to a plug flow in the reactor. The combustion reactants are, however, introduced continuously throughout the reactor, adding up to a total volumetric flow of 2 cm^3/s. In Table 4.3, the inlet conditions for the simulations are presented.

Table 4.3: Inlet conditions for the simulations investigating the environment in a CLC-unit using CO/CO_2 and H_2/H_2O to determine the reduction potential and some introduced activity.

Inlet 1					**Inlet 2**		
$\mathbf{x}_{CO}$	$\mathbf{x}_{CO_2}$	$\mathbf{x}_{H_2}$	$\mathbf{x}_{H_2O}$	$\mathbf{x}_{NH_3}$	$\mathbf{x}_{CO}$	$\mathbf{x}_{H_2}$	$\mathbf{x}_{O_2}$
0-0.895	0.990-0.095	-	-	0.010	0.330	0.330	0.330
-	-	0-0.895	0.990-0.095	0.010	0.330	0.330	0.330

To evaluate the catalytic impact on the gas-phase reactions described in Section 2.6, simulations corresponding to experiments from previous work conducted by Mayrhuber [22] have been replicated with the constraint of only containing gas-phase modelling. Simulations describing this are presented in Table 4.4.

Table 4.4: Inlet conditions for the simulations investigating the gas-phase reactions in Equation (2.23) and (2.24).

$\mathbf{x}_{NH_3}$	$\mathbf{x}_{NO}$	$\mathbf{x}_{N_2}$
1.000	-	-
0.005	-	0.995
0.0033	0.0033	0.9934
0.0025	0.005	0.9925

4.2.2 Heterogeneous Reactions

To include the OC in the mechanism in CHEMKIN, the element Me and the species Me and MeO have been added where Me and MeO represent a generic reduced and oxidised OC, respectively. Note that MeO and Me are represented as gaseous compounds due to limitations of the software. Due to the result of the modelling of the homogeneous gas-phase reactions, see Section 5.1.1, only the reactor part that corresponds to the FB is modelled when incorporating heterogeneous reactions. The length of the reactor, z, is set to 22 mm and the temperatures that are investigated are 850 °C, 900 °C and 950 °C, and the other operating conditions are the same as stated in Table 4.1.

Kinetic parameters are fitted to previous experimental results obtained from Cheng et al. [23] and Neumann [21], with the constraint of only including the catalytic decomposition of NH_3 (Equation (2.23)), the oxidation of NH_3 into NO (Equation (2.20)) and the reduction of NO to N_2 (Equation (2.22)). All reactions are considered first order with respect to the gaseous compound and the rate constants are based on the Arrhenius equation (Equation (2.29)). To obtain kinetic parameters for the catalytic decomposition of NH_3, data obtained from the work by Cheng et al. [23] is used. They performed experiments in an empty reactor and experiments with sea sand as bed material, with the result of sea sand having slightly higher NH_3 conversion than empty reactor experiments. Assuming that the OC possesses

some catalytic effects but not as high as sea sand, the kinetic parameters are derived for values in between empty reactor experiments and sea sand experiments. Furthermore, the oxidation of NH_3 and reduction of NO are investigated using data from the work by Neumann [21] with the simplification that NO_2 is counted as NO. Neumann [21] reported small fractions of NO_2. The kinetic parameters for the oxidation of NH_3 is obtained by fitting the kinetic parameters to have the same amount of remaining NH_3 as in the experiments. For the highest temperature investigated, no NH_3 was found in the outlet gas. In that case, the model assumes an NH_3 concentration profile which takes positive values until the reactor outlet, where it is zero. Thereafter, the reduction of NO is included to the model by fitting the experimental outlet concentrations of NO and N_2, respectively. The OC used in the work by Neumann [21] is an Australian sand ilmenite which has been calcinated, i.e. heat treated.

4.3 Experimental

In the following section, details regarding the experimental part, such as pre-treatment of the OC and operating conditions of the TGA, are presented.

4.3.1 Oxygen Carrier - Pre-Treatment and Activation

The used oxygen carrier is a Norwegian rock ilmenite. Before usage, the ilmenite is pre-treated by heating and sieving. The heat treatment is conducted in order to increase the strength of the OC and also to stabilise the structure. Further, it removes moisture and potential volatile impurities. The heat treatment is performed by placing a sample of fresh ilmenite inside a furnace, for which the temperature is increased 100 °C/h until 950 °C is reached, followed by 24 hours of constant temperature. The dried sample is thereafter sieved to a particle size of 125-180 µm.

With fresh ilmenite, the fuel conversion has shown to vary greatly between cycles [64]. To avoid this and to stabilise the reactivity, ilmenite is activated by undergoing multiple redox cycles until the fuel conversion is stabilised [64]. The redox cycle consists of an altering gas flow consisting of either syngas (50 % CO in H_2) or diluted air (5 % O_2 in N_2). Between the oxidation and the reduction, an inert phase of N_2 is passed through the reactor according to operating conditions in Table 4.5. The reactor is operated as a FB at 850 °C with a flow rate of 800 ml/min for all phases. For a description regarding the reactor setup, see Appendix B.

Table 4.5: Details on activation cycles of fresh ilmenite.

Phase	Gas	Time (s)
Oxidation	Diluted air (5 % O_2 in N_2)	Until full oxidation of OC
Inert	N_2	60
Reduction	Syngas (50 % CO in H_2)	20

4.3.2 Thermal Gravimetric Analysis - TGA

The oxidation of NH_3 and the reduction of NO with ilmenite are investigated using TGA. The main objective of TGA is to measure a mass change during a time interval and/or a temperature interval [65]. TGA has been used in previous studies [33, 59, 60, 66–68] to obtain kinetics relevant to CLC. The advantage of using a TGA compared to a FB setup when determining kinetics is that gas bypass through bubble formation is avoided.

The experiments are conducted in a Q500 from TA Instruments, with an alumina crucible. Samples of activated and oxidised ilmenite with the mass 12.15 $\pm$0.45 mg are placed in a thin, evenly distributed layer in the crucible to minimise mass transfer resistance through the sample. Each sample of ilmenite is replaced after every full cycle. One full cycle consists of one oxidation and one reduction respectively at 850 °C, 900 °C and 950 °C. The concentration of each phase is kept constant during a full cycle. To study the reactions in Equation (2.20) and (2.22), the species NH_3 and NO are used respectively. Every full cycle is repeated for three concentrations of NH_3 and NO, see Table 4.6 for gas concentrations. During start-up, the temperature is increased by 10 °C/min and is thereafter kept constant during one redox cycle at all investigated temperatures. A set flow of 90 ml/min is used during all phases and 5 min of inert phase is introduced between each oxidation phase and reduction phase to hinder mixing between phases in the TGA furnace. The time for each oxidation and reduction phase is decided based on their mass weight and is manually supervised and altered as needed. During the experiments, the mass varies in the interval 97 % to 100 % of its fully oxidised weight, i.e. only a small fraction of the total mass is changed during the redox cycles.

Table 4.6: Gas concentrations during TGA measurements for the oxidation of NH_3 and reduction of NO respectively.

Phase	Reduction of ilmenite	Oxidation of ilmenite
Reduction	0.25/0.5/1 % NH_3 in N_2	10 % Syngas (50 % CO in H_2)
Inert	N_2	N_2
Oxidation	5 % O_2 in N_2	3000/4000/5000 ppm NO in N_2
Inert	N_2	N_2

Furthermore, experiments are conducted in order to investigate a potential mass transport dependency, see Appendix E. For the experiments investigating the reduction of ilmenite with NH_3, the reaction for the used sample mass is shown to be, at least partially, controlled by kinetics rather than mass transport. However, for the oxidation of ilmenite with NO, the same extensive investigation is not conducted, resulting in that the same legitimacy of the used sample mass cannot be made.

4.3.3 Data Evaluation

It is assumed that the only reaction that occurs when using NH_3 as reducing gas in the TGA is the oxidation of NH_3 to NO (Equation (2.20)). Furthermore, the bulk concentration of NH_3 is considered equal to the inlet concentration of NH_3 and the possible reaction between the product NO and the ilmenite is assumed to be negligible due to the low concentrations of product NO. When oxidising ilmenite with NO, the only plausible reaction is Equation (2.22). Further oxidation of NO to is not expected. Neither is it expected that the formed product, N_2, is reactive in that environment. Note that the NO gas is diluted into rather small concentrations in N_2, resulting in that the small amounts of N_2 that forms during oxidation of ilmenite is not affecting the bulk concentration of N_2 to any extent. In similarity to in the work by Abad et al. [33], the oxygen transport capacity, R_o, is set to 3.3 % for activated ilmenite.

As a first basis, the shrinking core model is used to describe the gas-solid reactions. It has previously been used to describe gas-solid reactions under CLC conditions, still, it should be emphasised that it is an empirical model that simplifies a relatively complex phenomena. However, it was found that the shrinking core model does not fit the experimental results well when oxidising ilmenite with NO. Instead, a linear dependency seems to describe the relationship between the conversion level and the time in the region of interest with respect to CLC applications. The same results have been seen in previous studies [60, 66, 69], in which an empirical linear model was used according to:

$$\frac{dX}{dt} = \frac{1}{\tau}. \tag{4.1}$$

Equation (2.32) and (4.1) are integrated and the following equations are used for derivation of kinetic properties for the reduction of ilmenite with NH_3 and the oxidation of ilmenite NO respectively:

$$\frac{t}{\tau} = 1 - (1 - X_r)^{1/3} \tag{4.2}$$

and

$$\frac{t}{\tau} = X_o. \tag{4.3}$$

The equation describing the time for complete solid conversion, τ, is however modified with respect to the normal model (Equation (2.33)) to not contain any physical properties of the OC, and the reverse reaction is assumed to be negligible - resulting in the following expression:

$$\tau = \frac{1}{k' C^n}, \tag{4.4}$$

where k' is a modified rate constant. By rearranging Equation (4.4) and taking the logarithm of both sides, the following equation can be obtained:

$$\ln(\frac{1}{\tau}) = \ln(k') + n \ln(C). \tag{4.5}$$

Creating a plot with $\ln(\frac{1}{\tau})$ on the y-axis and $\ln(C)$ on the x-axis results in a graph with the slope corresponding to the reaction order. When the derived reaction orders depend on the temperature, the reaction order obtained for 950 °C is used. Furthermore, kinetic parameters can be derived from $\ln(k')$ as explained in Section 2.8.

5
Results

In this chapter the results from the detailed reaction modelling are presented followed by the results and the post processing of the experimental part of the thesis.

5.1 Detailed Reaction Modelling

The results of the detailed reaction modelling are divided into two parts; one with the original mechanism, i.e. only gas-phase reactions, and one with heterogeneous reactions added to the mechanism according to the reaction pathway model found in Section 4.1 and data from previous studies. From here on, NO_x is defined as NO and NO_2 while N_2O is reported separately.

5.1.1 Homogeneous Reactions

To investigate whether the reduction potential in the reactor could be modelled using CO and CO_2, simulations with only CO and CO_2 as reactants are performed. The simulations are conducted with an increased reduction potential of the environment and the result is presented in Figure 5.1, where the oxygen concentration is shown on the y-axis.

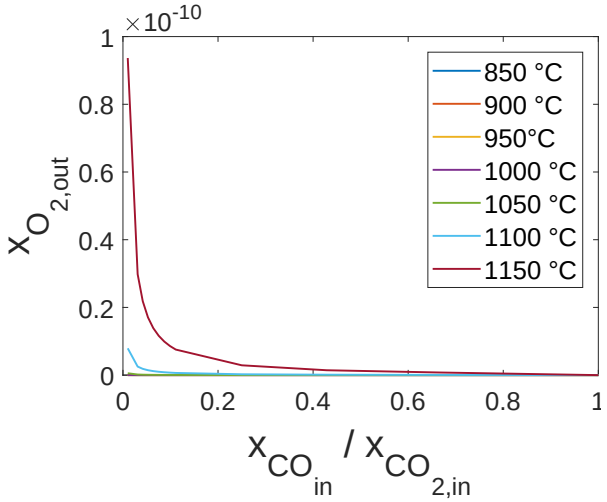

Figure 5.1: Outlet molar fraction of oxygen for a system with the reactants CO and CO_2 in different ratios.

To further examine how the reactor behaves when introducing a nitrogen species to the system, simulations with NH_3 as nitrogen species are performed in the same environment. The resulting NO_x concentration in the outlet of the reactor is presented in Figure 5.2. No significant amounts of NO_x nor N_2O are produced during these conditions. In Figure 5.3, the conversion to different nitrogen species is presented, including HCN and HCNO - common intermediates. At 850 °C, only a slight conversion of NH_3 occurs at high reduction potentials. At 1150 °C, however, the conversion of NH_3 is approximately 70-80 % towards either N_2, HCN or HNCO. The conversion toward N_2 is decreasing with an increased reduction potential. The same investigation is conducted for the inlet species H_2 and H_2O, with similar results as for the CO and CO_2 case, see Appendix C.

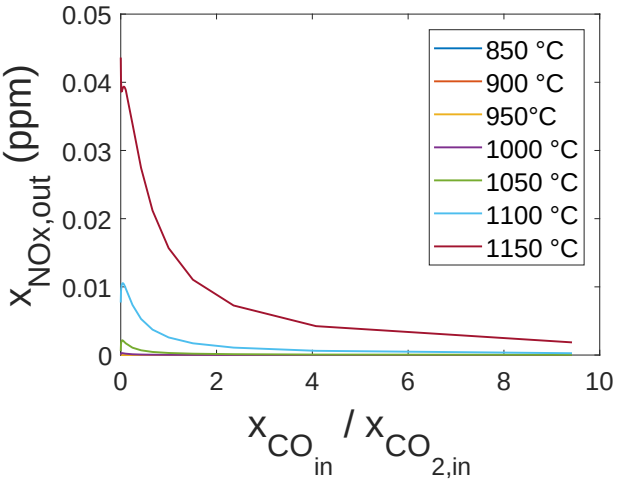

Figure 5.2: Outlet molar fraction of NO_x for a system with the reactants CO, CO_2 in different ratios and 1 % NH_3.

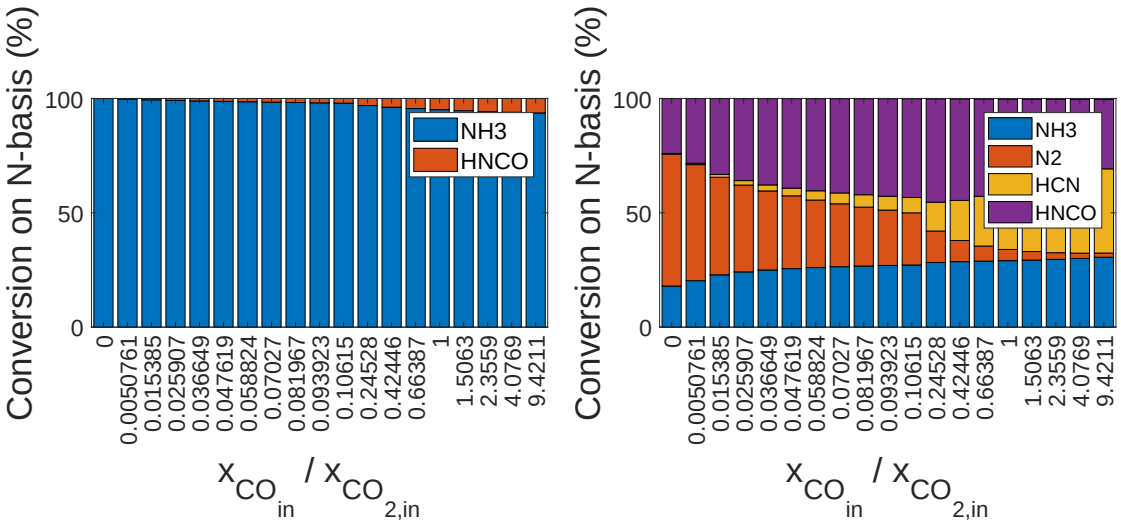

(a) **(b)**

Figure 5.3: Nitrogen conversion for a system with the reactants CO, CO_2 and 1 % NH_3 with varying inlet fractions of CO and CO_2 at (a) 850 °C and (b) 1150 °C.

When introducing some combustion activity to the system, i.e. combustion species, the outlet molar fraction of NO_x is increased, both in the environment of H_2/H_2O and CO/CO_2, see Figure 5.4, however, to a larger extent in the case of CO/CO_2. The corresponding nitrogen conversion is shown in Figure 5.5. In general, the majority of the introduced NH_3 is converted to N_2 regardless of the reduction potential CO/CO_2. However, it can be seen that a higher reduction potential at 850 °C results in some unconverted NH_3. For H_2/H_2O, a higher fraction of NH_3 is unconverted. At low reduction potentials, the majority of the introduced NH_3 is converted to N_2 at 850 °C. For the higher temperature, 1150 °C, a larger fraction of NH_3 is reacted to N_2 than at 850 °C, however a significant amount of NH_3 is still unconverted.

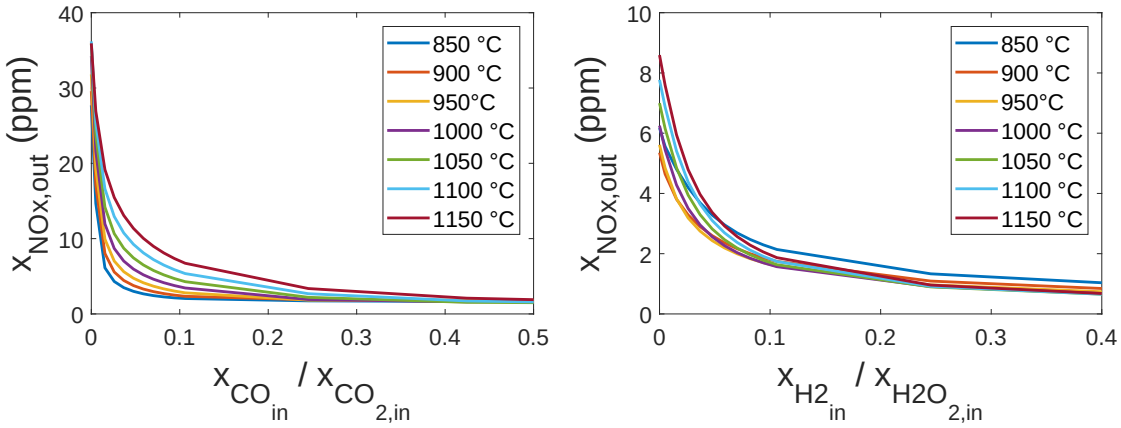

(a) **(b)**

Figure 5.4: Outlet molar fraction of NO_x for a system with the reactants (a) CO, CO_2 and NH_3 and (b) H_2, H_2O and NH_3, where combustion species are added throughout the reactor. Note, different scales on the y-axis.

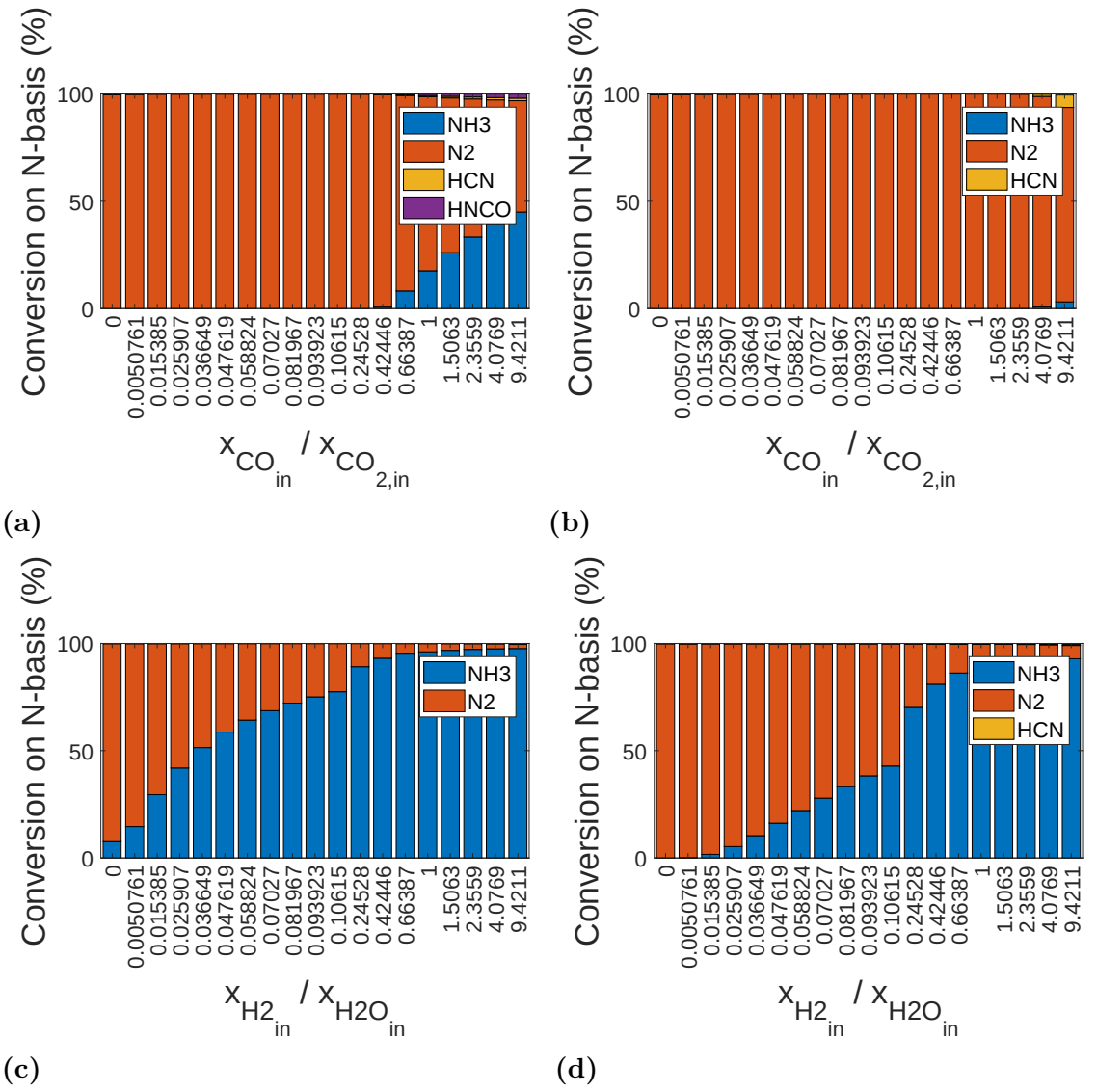

Figure 5.5: The nitrogen conversion for a system with the reactants CO, CO_2 and NH_3, where combustion species are added throughout the reactor at (a) 850 °C and (b) 1150 °C. The nitrogen conversion for a system with the reactants H_2, H_2O and NH_3, where combustion species are added throughout the reactor at (c) 850 °C and (d) 1150 °C.

Regarding the gas-phase reactions described in Equation (2.23) and (2.24) and the operating conditions in Table 4.4, no reactions seem to occur in the investigated temperature range (825-975 °C). None of the molar fractions of the nitrogen species change significantly in the simulations.

5.1.2 Heterogeneous Reactions

The kinetic parameters obtained from experimental data found in the literature for the catalytic decomposition of NH_3, the oxidation of NH_3 to NO by the OC and the reduction of NO to N_2 by the reduced OC are presented in Table 5.1. In

Figure 5.6, the N-conversions when including the different reactions in the original mechanism in CHEMKIN are presented. Data corresponding to the N-conversion presented in Figure 5.6a and Figure 5.6c are found in the work by Cheng et al. [23] and Neumann [21] respectively. The work by Cheng et al. [23] corresponds to the catalytic decomposition of NH_3 and the work by Neumann [21] corresponds to a batch reactor experiment with the inlet condition 1 % NH_3 in N_2. The N-conversion presented in Figure 5.6b is obtained from including the catalytic decomposition of NH_3 from Figure 5.6a and the oxidation of NH_3 to NO, fitted to obtain the total NH_3 conversion found in the work of Neumann [21].

The Me/MeO subset that has been included in the CHEMKIN mechanism is presented in Appendix C and corresponds to the kinetic parameters presented in Table 5.1.

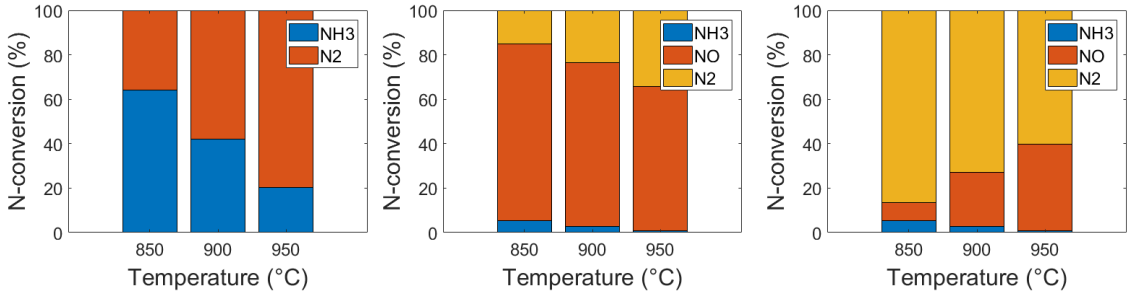

(a) **(b)** **(c)**

Figure 5.6: N-selectivity when incorporating (a) the catalytic decomposition of NH_3 (b) the catalytic decomposition of NH_3 and oxidation of NH_3 to NO and (c) the catalytic decomposition of NH_3, oxidation of NH_3 to NO and the reduction of NO to N_2.

Table 5.1: Details on kinetics for the catalytic decomposition of NH_3, oxidation of NH_3 to NO and the reduction of NO to N_2. The rate constants are given in (1/s) and the activation energies in (cal/mole).

Reaction	**Rate expression**	$\mathbf{k_0}$	$\mathbf{E_a}$
$2\,NH_3 \rightarrow N_2 + 3\,H_2$	$k[NH_3]$	$1.9 \cdot 10^6$	$3.5 \cdot 10^4$
$2\,NH_3 + 5\,MeO \rightarrow 2\,NO + 3\,H_2O + 5\,Me$	$k[NH_3]$	28.3	$6.4 \cdot 10^3$
$2\,NO + 2\,Me \rightarrow N_2 + 2\,MeO$	$k[NO]$	$6.9 \cdot 10^{-10}$	$-4.9 \cdot 10^4$

5.2 Experimental

In this section, results from the experimental part of the project are presented.

5.2.1 Reduction of Ilmenite with NH_3

Experiments are conducted for all combinations of investigated temperatures and concentrations of NH_3. In Figure 5.7, the concentration dependency is illustrated for all temperatures. The rate of reaction increases with increased concentration of NH_3 for all temperatures investigated. The temperature dependency is shown in Figure C.4 in Appendix C for all investigated concentrations of NH_3. A positive correlation between the rate of reaction and temperature at all concentrations of NH_3 is found.

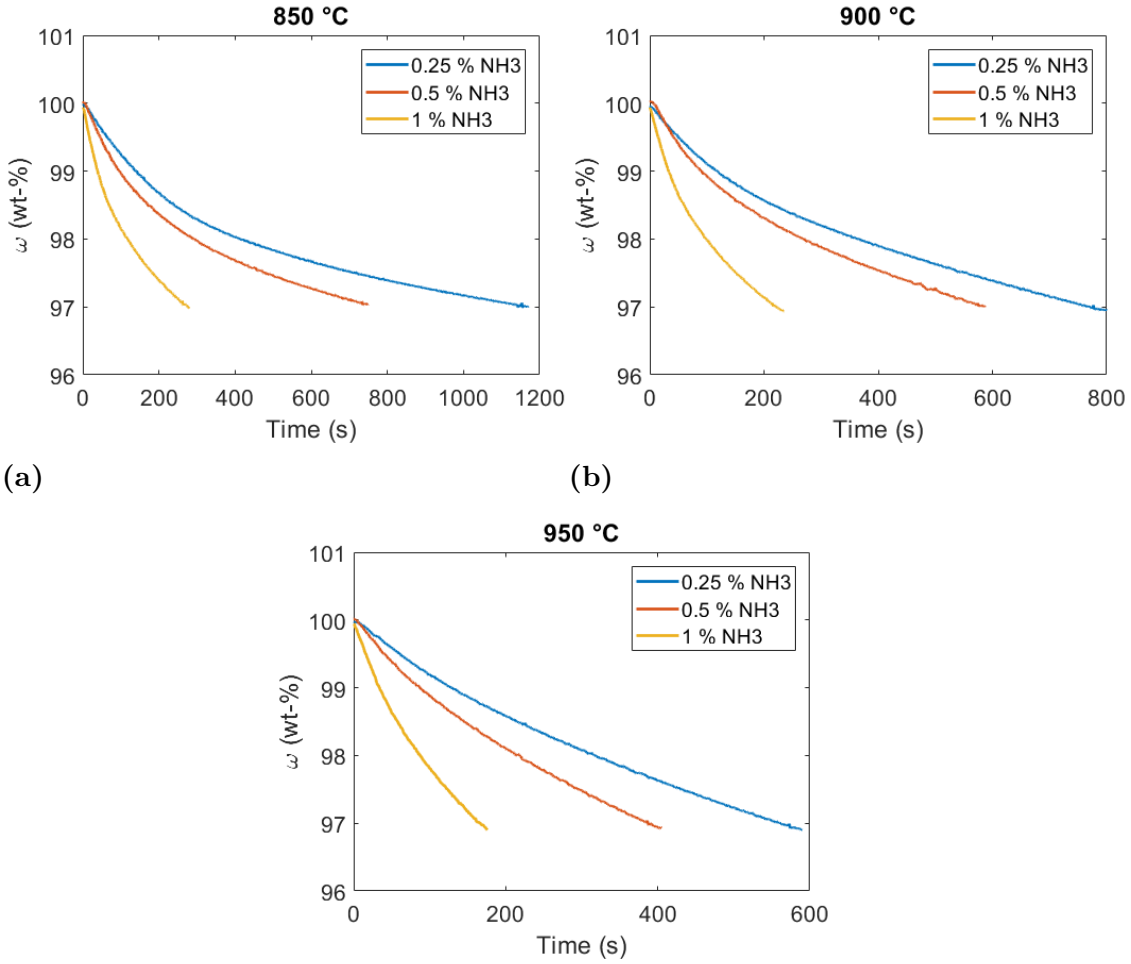

Figure 5.7: The mass-based OC conversion, ω, plotted against the time during the reduction of ilmenite with 0.25 %, 0.5 % and 1 % NH_3 at (a) 850 °C, (b) 900 °C and (c) 950 °C.

The experimental results of the reduction of ilmenite with NH_3 are fitted according to the shrinking core model, i.e. Equation (2.32), with τ calculated as expressed in Equation (4.4). The experimental values compared to the model predictions for all concentrations of NH_3 and the temperatures 850 °C and 950 °C are presented in Figure 5.8. The corresponding plot for the temperature 900 °C is shown in Figure C.5 in Appendix C. In general, the shrinking core model predicts the experimental

values well, especially at higher temperatures and at higher concentrations of NH_3.

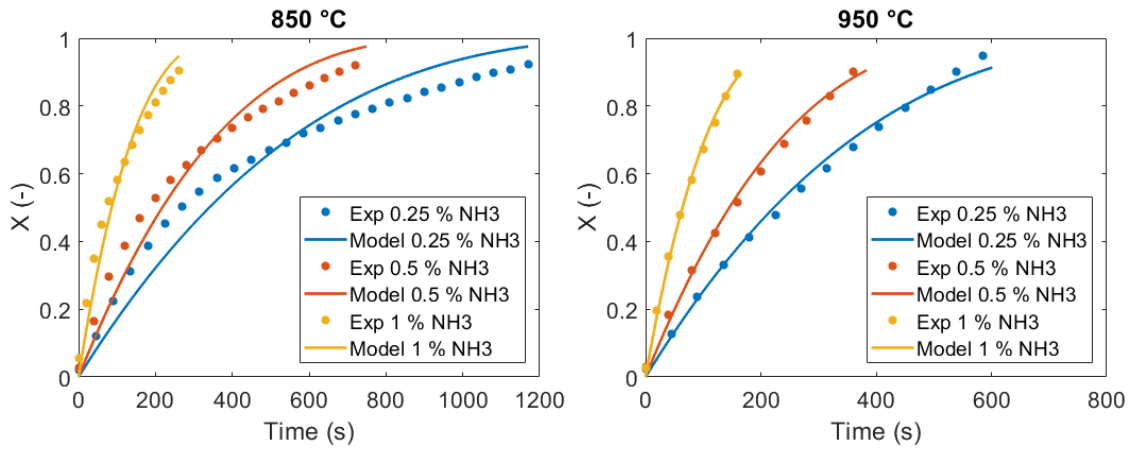

(a) **(b)**

Figure 5.8: Experimental values (Exp) and model predictions (Model) based on the shrinking core model of the solid conversion level, X, plotted against the time for the reduction of ilmenite with NH_3 at (a) 850 °C and (b) 950 °C.

Based on model parameters and experimental data, linear fits of $\ln(1/\tau)$ and $\ln(C)$ are conducted according to Equation (4.5), from which the order of reaction and the rate constant for the investigated temperatures are derived. In Figure 5.9a, the regression lines are plotted and in Figure 5.9b, the Arrhenius plot when using the order of reaction obtained from the reference temperature 950 °C is presented. In Table 5.2, the derived kinetic parameters are presented.

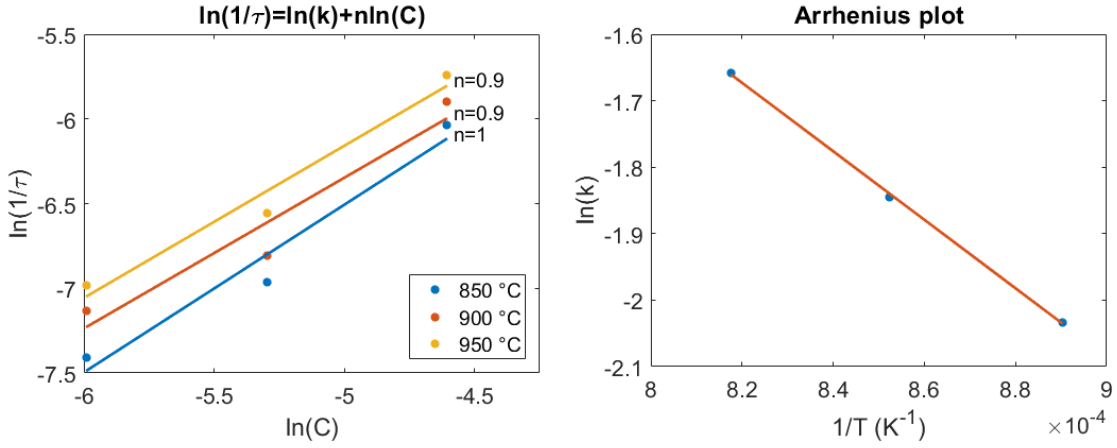

(a) **(b)**

Figure 5.9: (a) Regression lines of the relationship between $\ln(1/\tau)$ and $\ln(C_g)$ according to Equation (4.5). (b) Arrhenius plot for the reduction of ilmenite with NH_3.

Table 5.2: Kinetic parameters for the reduction of ilmenite with NH_3 based on experimental values and the shrinking core model, obtained from the Arrhenius plot in Figure 5.9b.

n	$\mathbf{k_0}$ **(m^{3n}mol^{-n}s^{-1})**	$\mathbf{E_a}$ **(cal/mole)**
0.9	12.83	$1.02{\cdot}10^4$

5.2.2 Oxidation of Ilmenite with NO

Experiments are conducted for all combinations of investigated temperatures and concentrations of NO. The result in terms of concentration dependency is presented in Figure 5.10. The rate of reaction is the highest at a gas-phase concentration of 5000 ppm NO, followed by 3000 ppm NO and lowest at 4000 ppm NO. At first, the rate of reaction is high. After this first period, the oxidation is continued at a constant lower rate until reaching close to full oxidation, where the rate is decreased further. The temperature dependency of the oxidation of ilmenite is illustrated in Figure C.7 in Appendix C for all investigated concentrations. The rate of reaction is decreasing with increased temperature for 3000 ppm NO and 5000 ppm NO. For 4000 ppm NO, the rate of reaction is fastest at 900 °C, followed by 850 °C and 950 °C.

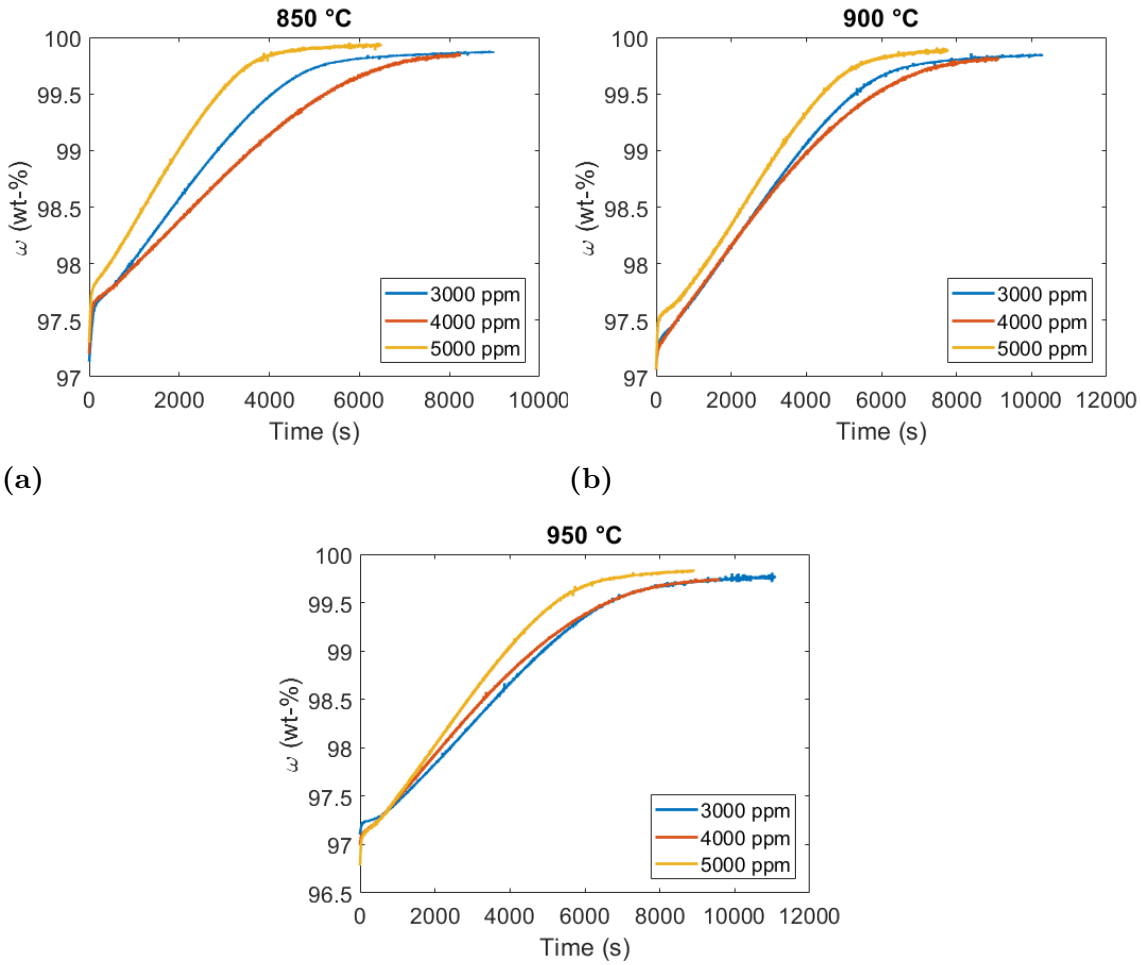

Figure 5.10: The mass-based OC conversion, ω, plotted against the time during the oxidation of ilmenite with 3000 ppm NO, 4000 ppm NO and 5000 ppm NO at (a) 850 °C, (b) 900 °C and (c) 950 °C.

The kinetic parameters are derived for the middle part of the oxidation, with regards to the intended use in a CLC system. In commercial applications of CLC, the OC would not be reduced with 3 wt-% from its fully oxidised level, but with a smaller fraction, necessary in order to avoid temperature drops in the fuel reactor. The shrinking core model did not fit the experimental values well and therefore, an empirical linear model to describe the relationship between the solid conversion level and the time is used according to Equation (4.1). The linear fitting alongside with the experimental values are presented in Figure 5.11 for 5000 ppm NO at 950 °C. The other combinations of concentrations and temperatures show a similar behaviour and can be found in Appendix C. The fittings are made in the solid conversion range of 0.4-0.8, with τ as expressed in Equation (4.4).

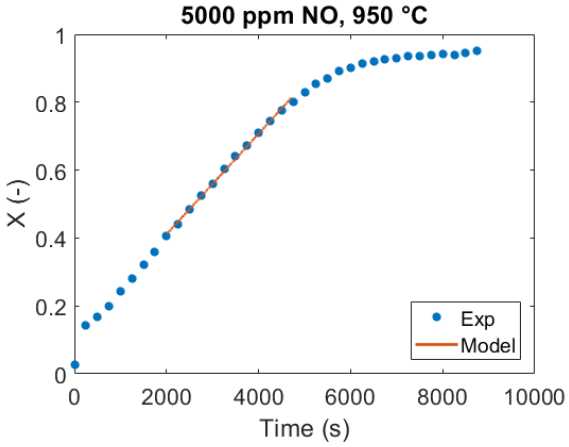

Figure 5.11: Experimental values (Exp) and model predictions (Model) based on a linear fitting of the solid conversion level, X, plotted against the time for the oxidation of ilmenite with 5000 ppm NO at 950 °C.

Based on model parameters and experimental data, the relationship between $\ln(1/\tau)$ and $\ln(C)$ is linearly fitted according to Equation (4.5), from which the order of reaction and the rate constant for the investigated temperatures are derived, see Figure 5.12a. Note that the linear regression has a large error margin. In Figure 5.12b, the Arrhenius plot when using the order of reaction obtained from the reference temperature 950 °C is presented. From the Arrhenius plot, the kinetic parameters are derived, see Table 5.3.

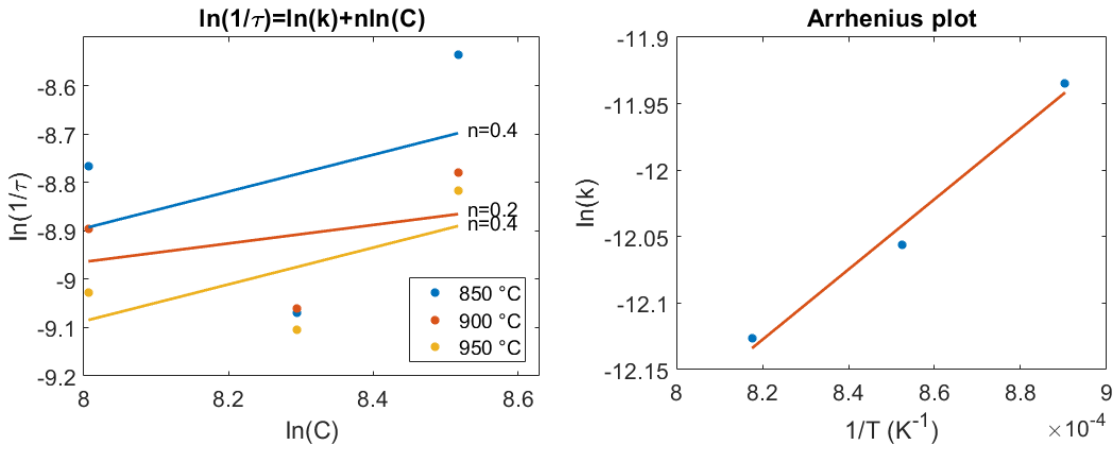

(a) **(b)**

Figure 5.12: (a) Regression lines of the relationship between $\ln(1/\tau)$ and $\ln(C_g)$ according to Equation (4.5). (b) Arrhenius plot for the oxidation of ilmenite with NO.

Table 5.3: Kinetic parameters for the oxidation of ilmenite with NO based on experimental values and a linear correlation, obtained from the Arrhenius plot in Figure 5.12b.

n	$\mathbf{k_0}$ **(m^{3n}mol^{-n}s^{-1})**	$\mathbf{E_a}$ **(cal/mole)**
0.4	$6.2{\cdot}10^{-7}$	$-5.25{\cdot}10^{3}$

Due to uncertainties in the experimental setup (see Section 6.3 and Appendix D), the kinetic parameters have been derived using only the experimental results from the oxidation of ilmenite with 5000 ppm NO, see Table 5.4. The order of reaction is assumed to be 0.4, as that is the derived order of reaction when deriving kinetics based on all concentrations of NO.

Table 5.4: Kinetic parameters for the oxidation of ilmenite with 5000 ppm NO based on experimental values and a linear correlation.

n	$\mathbf{k_0}$ **(m^{3n}mol^{-n}s^{-1})**	$\mathbf{E_a}$ **(cal/mole)**
0.4	$7.79{\cdot}10^{-6}$	$-7.72{\cdot}10^{3}$

5.2.2.1 First Regime of the Oxidation of Ilmenite

Two different rates are observed during the oxidation of ilmenite with NO. The rate during the first part of the oxidation with ilmenite based on the experiments shown in Figure 5.10 are presented in Table 5.5. During the first part of the oxidation the rate of reaction is significantly larger than during the middle part. The rate of reaction is decreasing with increased temperature and decreased concentration (with the exception of 4000 ppm at 950 °C). The corresponding ω values for the start point and end point in wt-% for the first regime, i.e. during the first rate of reaction, of the oxidation are presented in Table 5.6. Note that the oxidation of the ilmenite does not start at the same exact reduction level as it is manually controlled. When changing from reducing gases (syngas) to inert gas (N_2), there is a time delay where syngas is still reducing the OC. This time delay was hard to predict, resulting in slightly different starting values of the reduction potential.

Table 5.5: The rate of the oxidation of ilmenite with NO (wt-%/s) during the first regime.

Conc / **Temp**	**3000 ppm**	**4000 ppm**	**5000 ppm**
850 °C	0.0041	0.0044	0.0069
900 °C	0.0022	0.0036	0.0067
950 °C	0.0020	0.0016	0.0065

Table 5.6: Starting point of ω (wt-%)/ Ending point of ω (wt-%) during the first regime of the oxidation of ilmenite with NO.

Temp \ Conc	3000 ppm	4000 ppm	5000 ppm
850 °C	97.1/97.6	97.2/97.6	97.2/97.7
900 °C	97.1/97.3	97.1/97.2	97.0/97.4
950 °C	97.1/92.2	97.0/97.1	96.7/97.0

To investigate the first, rapid, part of the oxidation of ilmenite with NO further, the sample was reduced to different levels of wt-% of its fully oxidised level, see Figure 5.13. The lower degree of reduction that the oxidation starts at, the larger increase in wt-% is obtained immediately followed by the introduction of the oxidising gas NO. When the oxidation starts at values of ω greater than 98 wt-%, no significant difference in rate of reaction is observed, i.e. only one, constant, rate of reaction is observed.

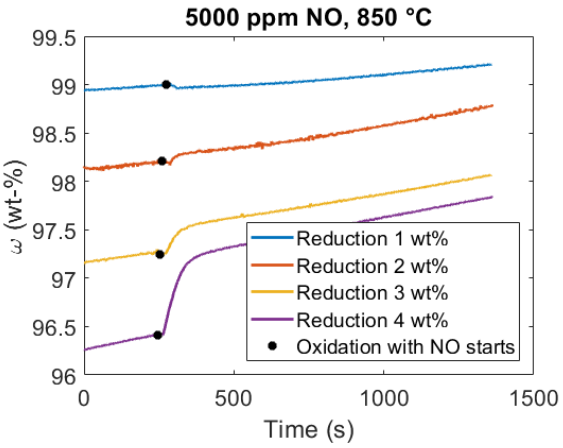

Figure 5.13: Oxidation of ilmenite with 5000 ppm NO at 850 °C, starting at different reduction levels.

6
Discussion

There is a very limited understanding of the fate of fuel nitrogen in CLC. The aim of this work is to increase the understanding of the process, something which has been done by synthesising relevant literature, extracting kinetic parameters from literature, conducting comprehensive gas-phase modelling and studying the important reactions experimentally. In this section, the results obtained from the modelling, including a detailed heterogeneous reactions pathway, and experimental work of this thesis are discussed. An analysis of the validity of the results and the used method is presented followed by suggestions on future research related to this thesis.

6.1 Detailed Reaction Modelling

From the modelling of the system consisting of CO and CO_2 in different ratios, it is clear that only a small fraction of molecular oxygen is found freely in the gas phase in the outlet of the reactor regardless of temperature and ratio of the inlet species. Furthermore, if NH_3 is added to the inlet, only small amounts of NO_x are formed at temperatures relevant to CLC, and the nitrogen conversion seen is not corresponding to NO_x formation reported in the literature for experiments under CLC conditions. Introducing combustion species to the system, NO_x formation is enhanced, however, still not close to the reported formation ratios. This argues that the heterogeneous reactions are crucial to NO formation in CLC and that the gas-phase chemistry is not controlling the NO formation.

It is important to include the catalytic decomposition of NH_3 in the kinetic modelling to avoid the risk of overestimating other reactions. Experiments conducted in an empty reactor, i.e. without any OC, show an NH_3 decomposition according to Cheng et al. [23] and Mayrhuber [22]. The finding that nothing notable occurs when modelling the potential catalytic reactions described in Equation (2.23) and (2.24) with the constraint of only considering gas-phase reactions supports the hypothesis of both Cheng et al. and Mayrhuber. To explain the behaviour, they suggested that the quartz walls and the quartz filter found in the used batch reactors have a catalytic effect on NH_3 decomposition. However, at higher temperatures than the ones currently operated in CLC, the homogeneous gas-phase reactions may be of larger importance.

6.1.1 Heterogeneous Reaction Pathway

In conventional combustion, the gas-phase chemistry and the formation of radicals are of utter importance and in control of the reaction pathways. However, the modelling results of this thesis argue that the homogeneous gas-phase chemistry cannot be the cause of NO_x formation unless molecular oxygen is found freely in the gas phase. In CLC, when using an OC without CLOU-properties, only small amounts or no molecular oxygen is expected in the gas phase. The natural path for formation of O-based radicals is therefore not existing in CLC. If O-based radicals were to be formed in CLC, they would be initiated from the lattice oxygen in the OC. However, surfaces are expected to quench radicals, which makes it hard to believe that they also would be the reason for chain initiation. Even if the OC could initiate radical formation, the next question is whether the formed radicals could avoid chain termination long enough to react with N-species in the gas phase. It does not seem feasible to produce radicals that are present in the gas phase in CLC.

Radicals could, however, still be a part of the reaction pathway. Pickering and Meites [70] describe possible approaches to heterogeneous redox reactions. The main idea for a heterogeneous gas-solid reaction to occur is adsorption of the gaseous reactant at the gas-solid interface. One particular adsorption is chemisorption, which occurs when the adsorbate, i.e. the gaseous reactant, reacts with the surface it is adsorbed at. According to Pickering and Meites [70], it is possible for the adsorbate to dissociate into radicals which are bound to the surface. Assuming that the adsorbate is binding in to an active site, which also could be reactive, proceeding reactions between the dissociated adsorbate and the solid could be initiated. To concretise this procedure, let's think of the oxidation of NH_3. NH_3 would be adsorbed onto the OC, to places which not only would work as an active site for catalysis, but also as a reactive site to enable a gas-solid reaction. Hence, for them to be reactive with NH_3, these sites would need to have available lattice oxygen. During this chemisorption, both O-based and N-based radicals are possible to form. In general, radicals are highly reactive, which would initiate reactions until a stable product is formed and desorbed. Since it is unlikely that one active site only provides enough oxygen for one reaction, the proceeding reactions are not necessarily occurring in consecutive order - based on what N-based radical and O-based radical that are formed. Instead a larger pool of bounded radicals could form in a complex, allowing radicals from different chain reactions to interact. Assuming that the chain reactions have a similar reaction pathway in the formed gas-radical-solid complex as in conventional gas-phase nitrogen chemistry, see Figure 2.2, NO and N_2 would be the expected stable N-products. In similarity to the gas-phase nitrogen chemistry, the selectivity of the two plausible products could be dependent on the concentration of different radicals in the formed radical pool. Thus, the well-established nitrogen chemistry for the gas phase could still be valid in heterogeneous reactions with some modifications to reaction rates due to the radical-solid bonds. A similar overall reaction mechanism, for the reaction of NH_3 to NO and N_2, is proposed by Thengane et al. [56]. However, they did not discuss the intermediate products or how the intermediate reactions proceed. They proposed that NH_3 would be absorbed on the surface of the metal oxide, enabling reactions with the lattice oxygen followed

by intermediate reactions to produce either NO or N_2, depending on the amount of available lattice oxygen and temperature. In conventional combustion, both the amount of oxygen and the temperature influence the distribution of radicals, which affect the selectivity towards NO or N_2. If the reactions regarding NH_3 oxidation in CLC were controlled by radical formation, the selectivity towards NO and N_2 could be, in similarity to the findings of Thengane et al. [56] and to the well-established gas-phase reaction pathways, influenced both by the amount of available lattice oxygen and the temperature. Both these parameters are expected to affect the radical concentration in the formed radical pool bound to the OC.

For the reduction of NO, the active sites are probably oxygen vacancies. One plausible reaction pathway is that the OC acts as a catalyst, enabling the adsorption of NO onto sites that correspond to oxygen vacancies. In catalysis, the reactant is adsorbed on the catalyst, where the catalyst breaks required bonds of the adsorbed reactant, enabling easier reaction followed by a desorption of the formed product [71]. Thus, the catalytic properties of the OC could break the bond in NO, which allows further reactions into the stable N-product N_2 and lattice oxygen, where N_2 is desorbed to the bulk.

6.2 Experimental

The results obtained from the experiments of reducing ilmenite with NH_3 are as expected; the rate of reaction is increased with increased temperature and concentration. The shrinking core model fits the experimental values acceptably well and a similar order of reaction is derived for all temperature, see Figure 5.9a.

The general trend when oxidising ilmenite with NO is that the oxidation rate decreases with increasing temperatures. This is not the expected result, as a temperature increase generally causes an increased rate of reaction. Furthermore, the concentration dependency of NO is ranking from 5000 to 3000 to 4000 ppm with respect to decreasing rate of reaction. It is expected that the highest concentration of NO would result in the highest reaction rate, but that the reaction is slower when oxidising with 4000 ppm NO compared to 3000 ppm NO is unexpected. However, an oxygen leak in the inert gas used to dilute the gases is suspected, see Appendix D, which could explain these results. For the highest concentration, the gas is not diluted with any external inert gas, while the lower concentrations are diluted with external inert gas that potentially contains some impurities. The lower concentration of NO, the larger fraction of external inert gas is used and, thus, fastening the reaction due to the oxygen leak. Due to the potential oxygen leak, the kinetic parameters have been derived both with respect to all concentrations and with respect to only the highest concentration. The rate constant is approximately one order of magnitude larger for the latter case, while the same order of reactions is assumed. The derived order of reaction could be underestimated since the rates of reaction for the oxidation of ilmenite with 4000 ppm and 3000 ppm NO could be overestimated due to the presence of oxygen. When deriving kinetic parameters based on only the 5000 ppm case, the rate constant will therefore be larger to compensate for the

reduced order of reaction. This is also in line with the observed results. However, the experiments are only conducted once for each operating condition, resulting in the need of repeated experiments to investigate this trend further.

During the oxidation of ilmenite with NO, two regimes with different rates of reaction was observed if the oxidation starts at ω-values of approximately 97 wt-%. During the first, rapid, part of the oxidation, the temperature seems to affect the oxidation to a larger extent than the concentration. In general, the same trend regarding the temperature dependency on oxidation rates is observed in both regimes; a slower oxidation with higher temperature. The reason for this rapid weight gain is not determined. However, a theory is that a phase transition occurs. Ilmenite is expected to form intermediate states when being oxidised, see section 2.4.1. This could also explain the temperature dependency as the particles can have different structural characteristics at different temperatures. It could also be in the nature of ilmenite to exhibit a lowered rate of reaction at increased temperatures as the same behaviour is seen during the middle part of the oxidation with NO. A phase transition could also explain the concentration dependency, as ilmenite is oxidised to similar oxidation levels but with different rates at a specific temperature regardless of the concentration. Nevertheless, the first regime is not of importance considering the intended application, as only a small fraction of the OC would be reduced to a reduction potential that low in actual CLC operation. The majority of the OC particles would be reduced to a reduction level corresponding to the second regime observed during the oxidation, see Figure 5.10.

6.3 Method Reliability

During the experiment, it was observed that the sample gained weight during the inert phases when the weight should be at a stabilised level. This weight gain is ascribed to an oxidation of the material, see Appendix D for further elaboration. Only small amounts of oxygen are expected and is not assumed to affect the experiments substantially when ilmenite is reduced with NH_3. The reduction is relatively fast and the OC is assumed to have a higher selectivity towards NH_3 than O_2 at the operational conditions used. The decrease in reduction potential of the gas phase due to possible traces of oxygen is assumed to be negligible. During the slow oxidation of ilmenite with NO the reaction is expected to be influenced by the presence of oxygen, as oxygen and NO are competing about active sites on the OC. See Section 6.2 and Appendix D for discussion related to the impacts of having oxygen present in the gas mixture.

The derived rate constants based on batch reactor experiments found in literature and based on the experimental work conducted with TGA in this thesis cannot be directly compared as they are derived with respect to different rate expressions. Although the actual numbers cannot be compared, trends can be. The general trends are the same in both cases:

(i) The rate of reaction is decreasing with increased temperature for the oxidation of ilmenite with NO.
(ii) The rate of reaction is increasing with increased temperatures for the reduction of ilmenite with NH_3.
(iii) The rate constant is significantly larger for reduction of ilmenite with NH_3 compared to the oxidation of ilmenite with NO.

This also supports the use of the proposed reaction pathway model. One of the reactions that are excluded in the proposed reaction pathway model compared to the reactions presented in the literature (see Section 2.6) is the reduction of the OC by NH_3 with the product N_2. The result of neglecting this reaction, if it occurs, is that NO formation is overestimated. Consequently, that would also lead to an overestimation of NO reduction. When oxidising ilmenite with NO in the TGA, however, the actual amount of NO is known and, therefore, the reaction is not overestimated. In the batch reactor experiments that the derivation of kinetic parameters is based on, the reactions occur simultaneously as NH_3 is introduced as the nitrogen species, which could overestimate the reaction rates. Thus, that the same trends in reaction rates are observed supports the use of the reaction pathway model.

6.4 Future Research

First and foremost, the experimental setup should be investigated and improved in order to avoid an oxygen leak to the system. This can be done in different ways; using another TGA and using inert gas from a different source. The first in order to exclude the possibility of having a malfunctioning TGA and the latter in order to exclude the potential oxygen leak arising from the inert gas source. Using another inert gas than N_2, for example Ar, is also favourable in order to exclude any potential driving forces due thermodynamic equilibrium between the reactive nitrogen species and inert N_2. All experiments conducted within this thesis need to be repeated to ensure a statistical significance of the kinetic parameters as the experiments only were conducted once at each operating condition.

Furthermore, to investigate the mechanism controlling the different rates of reaction obtained when oxidising ilmenite with NO, the reduction level of the OC before exposing it to NO should be controlled better. To do this, without manually monitoring the reduction level, H_2 and steam can be used as reducing gas instead of syngas. By changing the ratio between H_2 and steam, the reduction level of the OC can be controlled by thermodynamic limitations of the system. To further investigate this and to elaborate whether a phase transition is responsible for the change in reaction rate an elemental analysis, such as X-ray diffraction (XRD), should be conducted for ilmenite oxidised to different oxidation levels.

The derived kinetic parameters found in this thesis can be incorporated into existing, or future, models of a CLC-unit, for example in the model by Aronsson et al. [72]. By extending models to include the important reactions describing NO_x formation

and reduction, NO_x emissions can be predicted. The results can also be applied in processes related to OC, such as OCAC.

7
Conclusions

This study investigates the importance of homogeneous and heterogeneous reactions to NO_x formation in the fuel reactor in CLC. This was done by evaluating relevant literature, performing gas-phase modelling and conducting experiments using TGA followed by a kinetic evaluation.

The literature review shows that the operational setup affects the NO_x formation greatly, as almost no studies reported NO_x emissions from the fuel reactor in continuous CLC operation, while the opposite is applicable for experiments treating batch reactor experiments. The NO_x formation and reduction in batch reactor experiments are dependent on the type of OC and also the level of oxidation of the OC.

The detailed reaction modelling of gas-phase reactions argues that heterogeneous reactions seem to dominate the NO_x formation and reduction pathways, as the formed NO_x from experiments found in the literature cannot be ascribed the gas-phase reactions. This supports the proposed reaction pathway model, which has a large focus on the heterogeneous reactions. The model suggests that NH_3 may be catalytically decomposed into N_2 or oxidised to NO. The formed NO can be reduced to N_2, either by the reduced OC or by NH_3 in a catalytic reaction.

The main conclusions of the experimental part of this thesis, investigating the heterogeneous reactions, are the following:

(i) The rate of reaction is decreasing with increased temperature for the oxidation of ilmenite with NO.
(ii) The rate of reaction is increasing with increased temperatures for the reduction of ilmenite with NH_3.
(iii) The rate constant is significantly larger for reduction of ilmenite with NH_3 compared to the oxidation of ilmenite with NO.

These findings implicate that NO is produced faster than it is consumed, resulting in that NO emissions are expected. Furthermore, an increased temperature results in both higher NO formation and lower NO reduction, leading to an increased selectivity towards NO compared to N_2 when increasing the temperature. Finally, the results of this thesis clearly show the importance of OC material with respect to nitrogen chemistry, where it is clear that both the heterogeneous reduction and oxidation reactions are important.

Bibliography

[1] European Commission. Paris Agreement [Internet]. European Commission; [year unknown]. [cited 2018 Sep 24]. Available from: `https://ec.europa.eu/clima/policies/international/negotiations/paris_en`.

[2] Nandy A, Loha C, Gu S, Sarkar P, Karmakar M K, Chatterjee P K. Present status and overview of Chemical Looping Combustion technology. Renewable and Sustainable Energy Reviews. 2016;59:597-619.

[3] IPCC. IPCC Special Report on Carbon Dioxide Capture and Storage. Cambridge, United Kingdom and New York, NY, USA: Cambridge University Press; 2005.

[4] Adánez J, Abad A, Garcia-Labiano F, Gayan P, de Diego L F. Progress in Chemical-Looping Combustion and Reforming technologies. Progress in Energy and Combustion Science. 2012;38(2):215-82.

[5] Mendiara T, Gayán P, García-Labiano F, de Diego L F, Pérez-Astray A, Izquierdo M T, et al. Chemical looping combustion of biomass: an approach to BECCS. Energy Procedia. 2017;114:6021-9.

[6] Rhodes J.S., Keith D.W. Biomass with capture: negative emissions within social and environmental constraints: an editorial comment. Climatic Change. 2008;87(3-4):321–8.

[7] Gough C, Upham P. Biomass energy with carbon capture and storage (BECCS or Bio-CCS). Greenhouse Gases Science and Technology. 2011;1(4):324-34.

[8] EPA. Nitrogen Oxides (NO_x), Why and How They Are Controlled. Washington, DC, USA: U.S. Environmental Protection Agency; 1999.

[9] EPA. Methane and Nitrous Oxide Emissions from Natural Sources. Washington, DC, USA: U.S. Environmental Protection Agency; 2010.

[10] Mendiara T, Izquierdo M T, Abad A, de Diego L F, García-Labiano F, Gayán P, et al. Release of pollutant components in CLC of lignite. International Journal of Greenhouse Gas Control. 2014;22:15-24.

[11] Miller J.A., Bowman C. T. Mechanism and modeling of nitrogen chemistry in combustion. Progress in Energy and Combustion Science. 1989;15(4):287-338.

[12] Jensen A, Johnsson J.A., Andries J, Laughlin K, Read G, Mayer M, et al. Formation and reduction of NO_x in pressurized fluidized bed combustion of coal. Fuel. 1995;74(11):1555-69.

[13] Markström P, Linderholm C, Lyngfelt A. Chemical-looping combustion of solid fuels - Design and operation of a 100 kW unit with bituminous coal. International Journal of Greenhouse Gas Control. 2013;15:150-62.

[14] Gu H, Shen L, Zhong Z, Niu X, Ge H, Zhou Y, et al. NO release during chemical looping combustion with iron ore as an oxygen carrier. Chemical Engineering Journal. 2015;264:211-20.
[15] Linderholm C, Schmitz M, Knutsson P, Källén M, Lyngfelt A. Use of Low-Volatile Solid Fuels in a 100 kW Chemical-Looping Combustor. Energy Fuels. 2014;28(9):5942-52.
[16] Song T, Shen L, Xiao J, Chen D, Gu H, Zhang S. Nitrogen transfer of fuel-N in chemical looping combustion. Combustion and Flame. 2012;159(3):1286-95.
[17] Linderholm C, Knutsson P, Schimtz M, Markström P, Lyngfelt A. Material balances of carbon, sulfur, nitrogen and ilmenite in a 100 kW CLC reactor system. International Journal of Greenhouse Gas Control. 2014;27:188-202.
[18] Bayham S.C., Kim H.R., Wang D, Tong A, Zeng L, McGiveron O, et al. Iron-Based Coal Direct Chemical Looping Combustion Process: 200-h Continuous Operation of a 25-kW_{th} Subpilot Unit. Energy Fuels. 2013;27(3):1347-56.
[19] Song T, Shen T, Shen L, Xiao J, Gu H, Zhang S. Evaluation of hematite oxygen carrier in chemical-looping combustion of coal. Fuel. 2013;104:244-52.
[20] Wismer A. Influence of Oxygen Carrier Conversion and Syngas Concentration on NO_x Formation in Chemical-Looping Combustion [master's thesis]. Gothenburg: Chalmers University of Technology; 2016.
[21] Neumann N. NO_x Formation in Chemical-Looping Combustion [master's thesis]. Gothenburg: Chalmers University of Technology; 2014.
[22] Mayrhuber S. Effect of Oxygen Carrier on NO_x Formation. Gothenburg: Chalmers University of Technology; 2018.
[23] Cheng M, Normann F, Zhao D, Li Z, Cai N, Leion H. Oxidation of Ammonia by Ilmenite under Conditions Relevant to Chemical-Looping Combustion. Energy Fuels. 2015;29(12):8126-34.
[24] Östergren M. NO_x Formation in Chemical Looping Combustion with Solid Fuel [master's thesis]. Gothenburg: Chalmers University of Technology; 2015.
[25] Normann F, Cheng M, Zhao D, Li Z, Cai N, Leion H. Oxidation of ammonia over a copper oxide-containing solid oxygen carrier with oxygen uncoupling capability. Combustion and Flame. 2016;165:445-52.
[26] Leung D.Y.C., Caramanna G, Maroto-Valer M.M. An overview of current status of carbon dioxide capture and storage technologies. Renewable and Sustainable Energy Reviews. 2014;39:426-43.
[27] Hossain M.M., de Lasa H.I. Chemical-looping combustionn (CLC) for inherent CO_2 separations - a review. Chemical Engineering Science. 2008;63(18):4433-51.
[28] de Diego L.F., García-Labiano F, Adánez J, Gayán P, Abad A, Corbella B.M., et al. Development of Cu-based oxygen carriers for chemical-looping combustion. Fuel. 2004;83(13):1749-57.
[29] Skulimowska A, Di Felice L, Kamińska-Pietrzak N, Celińska A, Pławecka M, Hercog J, et al. Chemical looping with oxygen uncoupling (CLOU) and chemical looping combustion (CLC) using copper-enriched oxygen carriers supported on fly ash. Fuel Processing Technology. 2017;168:123-30.
[30] Mattisson T. Materials for Chemical-Looping with Oxygen Uncoupling. ISRN Chemical Engineering. 2013;2013.

[31] Adánez J, de Diego L.F., García-Labiano F, Gayán P, Abad A. Selection of Oxygen Carriers for Chemical-Looping Combustion. Energy Fuels. 2003;18(2):371-7.
[32] Mattisson T, Järdnäs A, Lyngfelt A. Reactivity of Some Metal Oxides Supported on Alumina with Alternating Methane and Oxygen - Application for Chemical-Looping Combustion. Energy Fuels. 2003;17(3):643-51.
[33] Abad A, Adánez J, Cuadrat A, García-Labiano F, Gayán P, de Diego L.F. Kinetics of redox reactions of ilmenite for chemical-looping combustion. Chemical Engineering Science. 2011;66(4):689-702.
[34] Leion H, Lyngfelt A, Johansson M, Jerdal E, Mattisson T. The use of ilmenite as an oxygen carrier in chemical-looping combustion. Chemical Engineering Research and Design. 2008;86(9):1017-26.
[35] Azis M.M., Jerndal E, Leion H, Mattisson T, Lyngfelt A. On the evaluation of synthetic and natural ilmenite using syngas as fuel in chemical-looping combustion (CLC). Chemical Engineering Research and Design. 2010;88(11):1505-14.
[36] Pour N, Zhao D, Schwebel G, Leion H, Lind F, Thunman H. Laboratory Fluidized Bed Testing of Ilmenite a Bed Material for Oxygen Carrier Aided Combustion (OCAC): In Proceedings of the 11th International Conference on Fluidized Bed Technology; 14-17 May 2014; Beijing, China.
[37] Thunman H, Lind F, Breitholtz C, Berguerand N, Seemann M. Using an oxygen-carrier as bed material for combustion of biomass in a 12-MW_{th} circulating fluidized-bed boiler. Fuel. 2013;113:300-9.
[38] Wang P, Leion H, Yang H. Oxygen-Carrier-Aided-Combustion in a Bench-Scale Fluidized Bed. Energy Fuels. 2017;31(6):6463-71.
[39] Glarborg P, Jensen A.D., Johnsson J.E. Fuel nitrogen conversion in solid fuel fired systems. Progress in Energy and Combustion Science. 2003;29(2):89-113.
[40] Keating E. L. Applied Combustion (Mechanical Engineering). 2nd ed. Boca Raton, Florida: CRC Press; 2007.
[41] Goldemberg J, editor. Interactions: Energy/Environment. Oxford, UK: EOLSS Publishers; 2009.
[42] Gómez-García M.A., Pitchon V, Kiennemann A. Pollution by nitrogen oxides: an approach to NO_x abatement using sorbing catalytic materials. Environment International. 2005;31(3):445-67.
[43] Johnsson J.E. Formation and reduction of nitrogen oxides in fluidized-bed combustion. Fuel. 1994;73(9):1398-415.
[44] Hämäläinen J.P., Aho M.J., Tummavuori J.L. Formation of nitrogen oxides from fuel-N through HCN and NH_3: a model-compound study. Fuel. 1994;73(12):1894-8.
[45] De Soete G.G. Overall reaction rates of NO and N_2 formation from fuel nitrogen. Symposium (International) on Combustion. 1975;15(1):1093-102.
[46] Löffler G, Andahazy D, Wartha C, Winter F, Hofbauer H. NO_x and N_2O Formation Mechanisms - A Detailed Chemical Kinetic Modeling Study on a Single Fuel Particle in a Laboratory-Scale Fluidized Bed. Journal of Energy Resources Technology. 2001;123(3):228-35.
[47] Kilpinen P, Kallio S, Konttinen J et al. Towards a quantitative understanding of NO_x and N_2O emission formation in full-scale circulating fluidised bed com-

bustors. In: Proceedings of the 16th International Conference on Fluidized Bed Combustion. May 13-16 2001. Reno, Nevada, USA; 2001.

[48] Heezius J. Investigation of LKAB magnetite ores ability to reduce NO_x emissions. Gothenburg: Chalmers University of Technology; 2019.

[49] Cooper D.A., Ljungström E.B. Decomposition of NH_3 over Quartz Sand at 840-960 °C. Energy Fuels. 1988;2(5):716-9.

[50] Bell T.E., Torrente-Murciano L. H_2 Production via Ammonia Decomposition Using Non-Noble Metal Catalysts: A Review. Topics in Catalysis. 2016;59(15-16):1438-57.

[51] Zhao J. Nitrogen Oxide Emissions from Circulating Fluidized Bed Combustion [dissertation on the Internet]. Vancouver: the University of British Columbia; 1992 [cited 2019 Feb 12]. Available from: `https://open.library.ubc.ca/cIRcle/collections/ubctheses/831/items/1.0058534`.

[52] Goel S. K., Morihara A, Tullin C, Sarafim A. F. Effect of NO and O_2 concentration on N_2O formation during coal combustion in a fluidized-bed combustor: Modeling results. 25th Symposium (International) on Combustion. 1994;25(1):1051-9.

[53] Jensen L. S. NO_x from cement production - reduction by primary measures [dissertation]. Copenhagen: Technical University of Denmark; 1999.

[54] Edland R. Modeling the Contributions of Volatile and Char-Bound Nitrogen to the Formation of NO_x Species in Iron Ore Rotary Kilns. Energy Fuels. 2018;32(2):2321-31.

[55] Mendiara T, Glarborg P. Ammonia chemistry in oxy-fuel combustion of methane. Combustion and Flame. 2009;156(10):1937-49.

[56] Thengane S.K., Bandyopadhyay S, Mitra S, Bhattacharya S, Hoadley A. An alternative process for nitric oxide and hydrogen production using metal oxides. Chemical Engineering Research and Design. 2016;112:36-45.

[57] Roberts G.W. Chemical Reactions and Chemical Reactors. Hoboken, New Jersey, USA: Wiley; 2008.

[58] Glarborg P, Bentzen L.L.B. Chemical Effects of a High CO_2 Concentration in Oxy-Fuel Combustion of Methane. Energy Fuels. 2008;22(1):291-6.

[59] Abad A, García-Labiano F, de Diego L.F., Gayán P, Adánez J. Reduction Kinetics of Cu-, Ni-, and Fe-Based Oxygen Carriers Using Syngas ($CO+H_2$) for Chemical-Looping Combustion. Energy Fuels. 2007;21(4):1843-53.

[60] Dueso C, Ortiz M, Abad A, García-Labiano F, de Diego L.F., Gayán P, et al. Reduction and oxidation kinetics of nickel-based oxygen-carriers for chemical-looping combustion and chemical-looping reforming. Chemical Engineering Journal. 2012;188:142-54.

[61] Sedor K.E., Hossain M.M., de Lasa H.I. Reduction kinetics of a fluidizable nickel-alumina oxygen carrier for chemical-looping combustion. The Canadian Journal of Chemical Engineering. 2008;86(3):323-34.

[62] Ahn H, Choi S. A comparison of the shrinking core model and the grain model for the iron ore pellet indurator simulation. Computers and Chemical Engineering. 2017;97:13-26.

[63] Rydén M, Hanning M, Corcoran A, Lind F. Oxygen Carrier Aided Combustion (OCAC) of Wood Chips in a Semi-Commercial Circulating Fluidized Bed Boiler Using Manganese Ore as Bed Material. Applied Sciences. 2016;6(11):347-66.

[64] Adánez J, Cuadrat A, Abad A, Gayán P, de Diego L.F., García-Labiano F. Ilmenite Activation during Consecutive Redox Cycles in Chemical-Looping Combustion. Energy Fuels. 2010;24(2):1402-13.

[65] Loganathan S, Valapa R.B., Mishra R.K., Pugazhenthi G, Thomas S. Thermal and Rheological Measurement Techniques for Nanomaterials Characterization. (2nd ed.) Amsterdam: Elsevier; 2017. Chapter 4, Thermogravimetric Analysis for Characterization of Nanomaterials; p. 67-108.

[66] Readman J.E., Olafsen A, Smith J.B., Blom R. Chemical Looping Combustion Using $NiO/NiAl_2O_4$: Mechanisms and Kinetics of Reduction - Oxidation (Red-Ox) Reactions from In Situ Powder X-ray Diffraction and Thermogravimetry Experiments. Energy Fuels. 2006;20(4):1382-7.

[67] Tijani M.M., Aqsha A, Mahinpey N. X-ray diffraction and TGA kinetic analyeses for chemical looping combustion applications. Data in Brief. 2018;17:200-9.

[68] Monazam E.R., Breault R.W., Siriwardane R, Miller D.D. Thermogravimetric Analysis of Modified Hematite by Methane (CH_4) for Chemical-Looping Combustion: A Global Kinetics Mechanism. Industrial & Engineering Chemistry Research. 2013;52(42):14808-16.

[69] Zafar Q, Abad A, Mattisson T, Gevert B, Strand M. Reduction and oxidation kinetics of $Mn_3O_{4/}Mg-ZrO_2$ oxygen carrier particles for chemical-looping combustion. Chemical Engineering Science. 2007;62(23):6556-67.

[70] Pickering W.F., Meites L. Heterogeneous Oxidation and Reduction Processes; Mechanisms and Analytical Applications. C R C Critical Reviews in Analytical Chemistry. 1973;3(3):271-297.

[71] Bligaard T, Nørskov J.K. Chemical Bonding at Surfaces and Interfaces. Amsterdam: Elsevier; 2008. Chapter 4, Heterogeneous Catalysis; p. 255-321.

[72] Aronsson J, Pallarès D, Lyngfelt A. Modeling and scale analysis of gaseous fuel reactors in chemical looping combustion systems. Particuology. 2017;35:31-41.

[73] Knutsson P, Linderholm C. Characterization of ilmenite used as oxygen carrier in a 100 kW chemical-looping combustor for solid fuels. Applied Energy. 2015;187:368-373.

A

Literature Review

In Table A.1, the results from the literature review regarding nitrogen chemistry in batch reactors are presented in tabular form. In Table A.2, the corresponding results regarding continuous operation of CLC are presented. The notation - means that information was not relevant (only applicable for the mass-based OC conversion ω) or not found in the literature.

Table A.1: A summary over the batch reactor experiments regarding nitrogen chemistry in CLC found in the literature.

Reference	**Oxygen Carrier**	ω	**Fuel**	**Temp (° C)**	**Inlet N-species**	**NO_x peak (ppm)**	**Selectivity (NH3/NOx/N2)**
Östergren [24][a]	60 % Fe_2O_3, 40 % Mg–ZrO_2	-	Swedish wood char	950	-	90	22/26/52
Östergren [24][a]	Ilmenite	-	Swedish wood char	950	-	55	14/33/53
Wismer [20]	60 % Fe_2O_3, 40 % Mg–ZrO_2	1/ 0.9927/ 0.9854/ 0.9821	25 vol% syngas	950	1 vol% NH_3	1060/ 800/ 270/ 0	-
Wismer [20]	40 % Mn_3O_4, 60 % Mg–ZeO_2	1/ 0.9899/ 0.9744/ 0.9713	25 vol% syngas	950	1 vol% NH_3	6000/ 6500/ 3500/ 0	-
Wismer [20]	40 % NiO, 60 % $NiAl_2O_4$	1/ 0.9682/ 0.9362	25 vol% syngas		1 vol% NH_3	25/ 25/ 25	-
Wismer [20]	60 % Fe_2O_3, 40 % Mg–ZrO_2	-	1/10/20/25 vol% syngas	950	0.5 vol% NH_3	1250/ 1750/ 1880/ 1880	-

Table A.1 continued from previous page

Wismer [20]	40 % Mn_3O_4, 60 % $Mg-ZrO_2$	-	1/10/20/25 vol% syngas	950	0.5 vol% NH_3	3900/ 4250/ 4500/ 4450	-
Cheng et al. [23]	Ilmenite	-	No fuel	850/ 900/ 950	1 vol% NH_3	2250/ 2250/ 2125	850 ° C: 1/17/82 900 ° C: 0/18/82 950 ° C: 0/18/82
Cheng et al. [23]	Ilmenite	-	No fuel	900	0.2/0.4/ 0.6/0.8/1 vol% NH_3	1500/ 2300/ 2500/ 3000/ 3400	0.2 vol% NH_3: 0/73/27 0.4 vol% NH_3: 0/58/42 0.6 vol% NH_3: 0/47/53 0.8 vol% NH_3: 0/43/57 1 vol% NH_3: 0/43/57
Neumann [21]	Calcinated ilmenite	-	No fuel	850/ 900/ 950	1 vol% NH_3	2000/ 3250/ 4500	850 ° C: 5/9/86 900 ° C: 3/27/70 950 ° C: 1/37/62
Neumann [21]	Calcinated ilmenite	-	50 vol% syngas	850	0.5 vol% NH_3	150	19/1/80
Neumann [21]	Calcinated ilmenite	-	40 vol% syngas	850	0.6 vol% NH_3	400	18/1/81
Neumann [21]	Calcinated ilmenite	-	20 vol% syngas	850	0.8 vol% NH_3	1600	13/3/84
Neumann [21]	Activated ilmenite	-	50 vol% syngas	850	0.5 vol% NH_3	2700	9/5/86
Neumann [21]	Activated ilmenite	-	40 vol% syngas	850	0.6 vol% NH_3	2750	2/6/92

Table A.1 continued from previous page

Neumann [21]	Activated ilmenite	-	30 vol% syngas	850	0.7 vol% NH_3	2500	2/6/92
Neumann [21]	Activated ilmenite	-	20 vol% syngas	850	0.8 vol% NH_3	3000	2/8/90
Neumann [21]	40 % CuO, 60 % ZrO_2	-	No fuel	850/ 900/ 950	1 vol% NH_3	4000/ 4500/ 3100	850 ° C: 0/28/72 900 ° C:0/43/57 950 ° C: 0/30/70
Neumann [21]	40 % CuO, 60 % ZrO_2	-	50 vol% syngas	900	0.5 vol% NH_3	2400	3/11/86
Neumann [21]	40 % CuO, 60 % ZrO_2	-	60 vol% syngas	900	0.4 vol% NH_3	1300	6/10/84
Normann et al. [25]	40 % CuO, 60 % ZrO_2	-	40 vol% syngas	900	0/0.05/ 0.1/0.3/0.6 vol% NH_3	2750/ 1625/ 750/ 500/ 0	0.05vol% NH_3: 0/67/33 0.1 vol% NH_3: 0/56/44 0.3 vol% NH_3: 0/40/60 0.6 vol% NH_3: 0/37/63
Normann et al. [25]	40 % CuO, 60 % ZrO_2	-	0/5/10/ 20/40 vol% syngas	900	0.6 vol% NH_3	-	0 vol% syngas: 0/50/50 5 vol% syngas: 0/48/52 10 vol% syngas: 0/46/54 20 vol% syngas: 0/43/57 40 vol% syngas: 0/36/64
Gu et al. [14][a]	83.08 wt-% Fe_2O_3	-	Bituminous coal	850/ 900/ 950/ 1000	1.03 % (ad)	20/ 35/ 45/ 45	-

Table A.1 continued from previous page

Gu et al. [14][b]	83.08 wt-% Fe_2O_3	-	Bituminous coal	850/ 900/ 950/ 1000	1.03 % (ad)	60/ 34/ 32/ 29	-
Gu et al. [14][a]	83.08 wt-% Fe_2O_3	-	Petcoke	850/ 900/ 950/ 1000	1.34 % (ad)	10/ 30/ 70/ 90	-
Gu et al. [14][b]	83.08 wt-% Fe_2O_3	-	Petcoke	850/ 900/ 950/ 1000	1.34 % (ad)	55/40/35/25	-
Mayrhuber [22]	Empty reactor	-	No fuel	825/ 875/ 925/ 975	0.33 % NH_3 + 0.33 % NO	2625/ 2700/ 2750/ 3000	825 °C: 36/35/29 875 °C: 32/39/29 925 °C: 32/40/28 975 °C: 32/46/22
Mayrhuber [22]	Empty reactor	-	No fuel	825/ 875/ 925/ 975	0.5 % NH_3 + 0.25 % NO	1600/ 790/ 260/ 290	825 °C: 35/19/46 875 °C: 65/7/28 925 °C: 28/2/70 975 °C: 28/3/69
Mayrhuber [22]	Empty reactor	-	25 % Syngas	825/ 875/ 925/ 975	0.25 % NO	1850/ 1625/ 1600/ 1490	825 °C: 4/71/25 875 °C: 5/55/40 925 °C: 3/58/39 975 °C: 3/53/44

Table A.1 continued from previous page

Mayrhuber [22]	Empty reactor	-	25 % Syngas	825/ 875/ 925/ 975	0.5 % NH_3	-	825 °C: 62/0/38 875 °C: 65/0/35 925 °C: 58/0/42 975 °C: 54/0/46
Mayrhuber [22]	Norweigan ilmenite	-	No fuel	825/ 875/ 925/ 975	0.5 % NH_3	580/ 480/ 390/ 280	-
Mayrhuber [22]	Norweigan ilmenite	0.9706 - 0.9926	No fuel	825/ 875/ 925/ 975	0.5 % NH_3	-	825 °C: -/0/- 875 °C:-/0/- 925 °C: -/0/- 975 °C: -/0/-
Mayrhuber [22]	Norweigan ilmenite	0.9945	No fuel	825/ 875/ 925/ 975	0.5 % NH_3	-	825 °C: -/0/- 875 °C:-/0.3/- 925 °C: -/0.7/- 975 °C: -/0/-
Mayrhuber [22]	Norweigan ilmenite	0.9963	No fuel	825/ 875/ 925/ 975	0.5 % NH_3	-	825 °C: -/0.9/- 875 °C:-/0.7/- 925 °C: -/0.6/- 975 °C: -/0/-
Mayrhuber [22]	Norweigan ilmenite	0.9981	No fuel	825/ 875/ 925/ 975	0.5 % NH_3	-	825 °C: -/4.3/- 875 °C:-/1.8/- 925 °C: -/0.5/- 975 °C: -/0/-

Table A.1 continued from previous page

Mayrhuber [22]	Norweigan ilmenite	0.9999	No fuel	825/ 875/ 925/ 975	0.5 % NH_3	-	825 °C: -/22/- 875 °C:-/18/- 925 °C: -/17/- 975 °C: -/14/-
Mayrhuber [22]	Norweigan ilmenite	0.9715 - 0.9918	25 % Syngas	825/ 875/ 925/ 975	0.5 % NH_3	-	825 °C: -/0/- 875 °C:-/0/- 925 °C: -/0/- 975 °C: -/0/-
Mayrhuber [22]	Norweigan ilmenite	0.9936	25 % Syngas	825/ 875/ 925/ 975	0.5 % NH_3	-	825 °C: -/2/- 875 °C:-/0.3/- 925 °C: -/0.4/- 975 °C: -/0.9/-
Mayrhuber [22]	Norweigan ilmenite	0.9954	25 % Syngas	825/ 875/ 925/ 975	0.5 % NH_3	-	825 °C: -/10/- 875 °C:-/3.2/- 925 °C: -/1.9/- 975 °C: -/2.5/-
Mayrhuber [22]	Norweigan ilmenite	0.9972	25 % Syngas	825/ 875/ 925/ 975	0.5 % NH_3	-	825 °C: -/27/- 875 °C:-/10/- 925 °C: -/6/- 975 °C: -/5/-
Mayrhuber [22]	Norweigan ilmenite	0.999	25 % Syngas	825/ 875/ 925/ 975	0.5 % NH_3	-	825 °C: -/49/- 875 °C:-/29/- 925 °C: -/17/- 975 °C: -/10/-

Table A.1 continued from previous page

Mayrhuber [22]	Norweigan ilmenite	-	25 % Syngas	825/ 875/ 925/ 975	0.5 % NH_3	-	825 °C: 1/5/94 875 °C: 0/3/97 925 °C: 0/1/99 975 °C: 0/1/99
Mayrhuber [22]	Norweigan ilmenite	0.9859 - 0.9982	No fuel	825/ 875/ 925/ 975	0.25 % NO	-	825 °C: -/0/- 875 °C:-/0/- 925 °C: -/0/- 975 °C: -/0/-
Mayrhuber [22]	Norweigan ilmenite	1	No fuel	825/ 875/ 925/ 975	0.25 % NO	-	825 °C: -/94/- 875 °C:-/98/- 925 °C: -/87/- 975 °C: -/88/-
Mayrhuber [22]	Norweigan ilmenite	0.9709 - 0.9921	25 % Syngas	825/ 875/ 925/ 975	0.25 % NO	-	825 °C: -/0/- 875 °C:-/0/- 925 °C: -/0/- 975 °C: -/0/-
Mayrhuber [22]	Norweigan ilmenite	0.9938	25 % Syngas	825/ 875/ 925/ 975	0.25 % NO	-	825 °C: -/4/- 875 °C:-/0.5/- 925 °C: -/0/- 975 °C: -/0.7/-
Mayrhuber [22]	Norweigan ilmenite	0.9956	25 % Syngas	825/ 875/ 925/ 975	0.25 % NO	-	825 °C: -/9/- 875 °C:-/2/- 925 °C: -/0/- 975 °C: -/2/-

Table A.1 continued from previous page

Mayrhuber [22]	Norweigan ilmenite	0.9973	25 % Syngas	825/ 875/ 925/ 975	0.25 % NO	-	825 °C: -/22/- 875 °C:-/9/- 925 °C: -/6/- 975 °C: -/3/-
Mayrhuber [22]	Norweigan ilmenite	0.9991	25 % Syngas	825/ 875/ 925/ 975	0.25 % NO	-	825 °C: -/44/- 875 °C:-/33/- 925 °C: -/13/- 975 °C: -/10/-
Mayrhuber [22]	Australian ilmenite	-	No fuel	825/ 875/ 925/ 975	1 % NH_3	1050/ 1000/ 750/ 900	-
Mayrhuber [22]	Australian ilmenite	-	25 % Syngas	825/ 875/ 925/ 975	0.5 % NH_3	-	825 °C: 3/8/89 875 °C:3/5/92 925 °C: 2/5/93 975 °C: 3/5/92
Mayrhuber [22]	Australian ilmenite	0.9716 - 0.9899	25 % Syngas	825/ 925	0.5 % NH_3	-	825 °C: -/0/- 925 °C: -/0/-
Mayrhuber [22]	Australian ilmenite	0.9917	25 % Syngas	825/925	0.5 % NH_3	-	825 °C: -/3.4/- 925 °C: -/2.7/-
Mayrhuber [22]	Australian ilmenite	0.9936	25 % Syngas	825/ 925	0.5 % NH_3	-	825 °C: -/9.3/- 925 °C: -/2.9/-
Mayrhuber [22]	Australian ilmenite	0.9954	25 % Syngas	825/ 925	0.5 % NH_3	-	825 °C: -/22/- 925 °C: -/6.7/-

Table A.1 continued from previous page

Mayrhuber [22]	Australian ilmenite	0.9973	25 % Syngas	825/ 925	0.5 % NH_3	-	825 °C: -/38/- 925 °C: -/15/-
Mayrhuber [22]	Australian ilmenite	0.9991	25 % Syngas	825/ 825	0.5 % NH_3	-	825 °C: -/51/- 925 °C: -/24/-

[a] H_2O as gasification medium
[b] CO_2 as gasification medium

Table A.2: A summary over the continuous operation of CLC regarding nitrogen chemistry found in the literature.

Reference	**Size (kW)**	**Oxygen Carrier**	**Temp (°C)**	**Fuel**	**Inlet N fraction**	**NO_x outlet (ppm)**	**N-conversion to NO_x**
Linderholm et al. [15]	100	Ilmenite	-	Swedish wood char	0.4 % daf[a]	500	-
Linderholm et al. [15]	100	Ilmenite	958.5/ 962	Mexican petroleum coke	1 % daf[a]	-	3-8 %/ 20 %
Mendiara et al. [10]	0.5	Ilmenite	875/ 930	Spanish lignite	0.6 %	-/ 75 mg/Nm^3	1 %
Gu et al. [14]	1	Fe_2O_3	880/ 905/ 930/ 955/ 980	Bituminous coal	1.03 % ad[b]	10/ 13/ 14/ 16/ 15	0.5-0.8 %
Song et al. [16]	1	NiO	850/ 880/ 920/ 950	Shenhua bituminous coal	1.03 % ad[b]	0/ 0/ 0/ 0	0 %
Song et al. [16]	1	NiO	850/ 880/ 920/ 950	Huaibei anthracite	1.39 % ad[b]	0/ 0/ 0/ 0	0 %
Linderholm et al. [17]	100	Ilmenite	-	Bituminous coal	-	-	5.6 %

Table A.2 continued from previous page

Bayham et al. [18]	25	Fe_2O_3	970	Sub-bituminous coal	-	1148-1669	10-15 %
Song et al. [19]	1	Fe_2O_3	970	Shenhua bituminous coal	1.03 % ad[b]	0	0 %
Song et al. [19]	1	Fe_2O_3	970	Huaibei anthracite	1.39 % ad[b]	0	0 %
Markström et al. [13]	100	Ilmenite	960	Bituminous coal	1.65 % daf[b]	1290	10-20 %
Mendiara et al. [5]	0.5	Iron ore	-	Pine sawdust	0.28 %	-	4-14 %
Mendiara et al. [5]	0.5	Iron ore	-	Olive stone	0.18 %	-	4-14 %
Mendiara et al. [5]	0.5	Iron ore	-	Almond shell	0.16 %	-	4-14 %

[a] ad = air-dried
[b] daf = dry and ash-free

B

Batch Reactor Setup

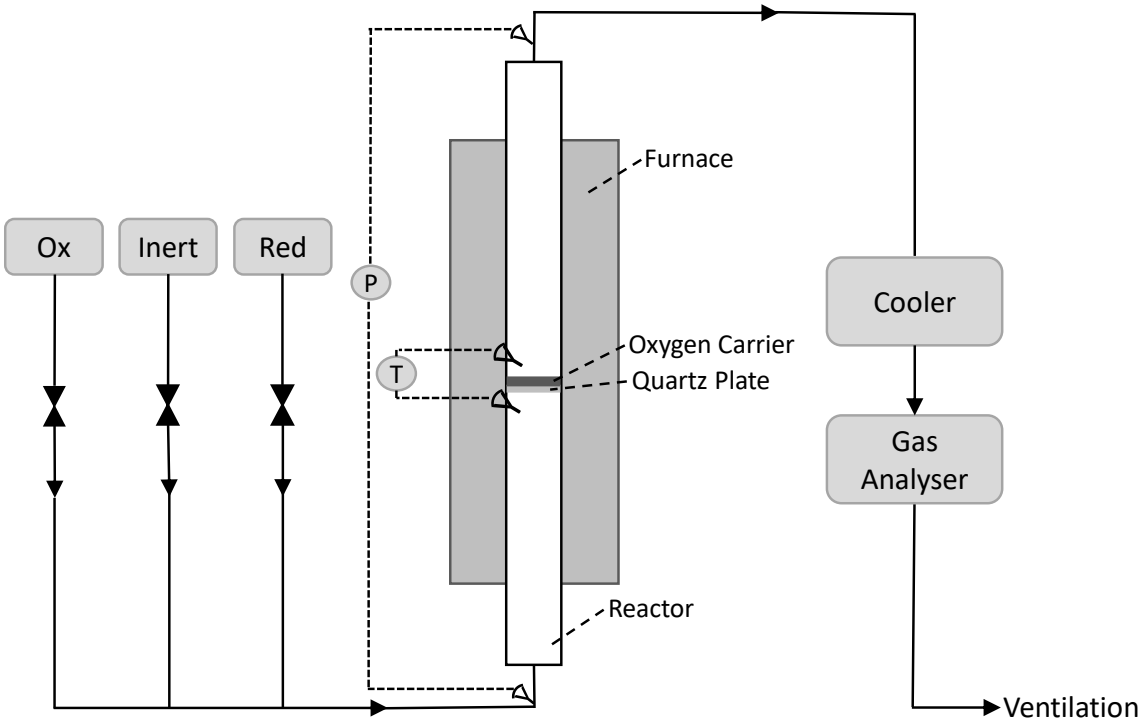

Figure B.1: The schematics for the reactor setup.

The reactor setup for the activation of ilmenite in a batch reactor is presented in Figure B.1. A quartz reactor with the length 780 mm and the inner diameter 22 mm is used both as air and fuel reactor in a CLC-unit by altering whether oxidising gases or reducing gases are passed through. The reactor is placed vertically inside a furnace with the gas fed from the bottom, allowing the reactor to be operated as a FB reactor. The OC is placed on a porous quartz plate, located 370 mm downstream from the reactor inlet. Two thermocouples, located 25 mm above and 5 mm below the quartz plate respectively, are used to measure the temperature. To ensure fluidisation, the pressure drop across the bed is measured. After passing the reactor, the flow is led through a cooler to remove moisture followed by a gas analyser. The gas analyser is a Rosemount™NGA 2000 Multi-Component Gas Analyzer.

C
Additional Results

C.1 Gas-Phase Modelling of the System H_2/H_2O in CHEMKIN

Simulations with H_2 and H_2O as reactants are conducted with an increased reduction potential of the environment, see Figure C.1. In similarity to when CO/CO_2 is used to vary the reduction potential, very small fractions of oxygen are found in the gas phase.

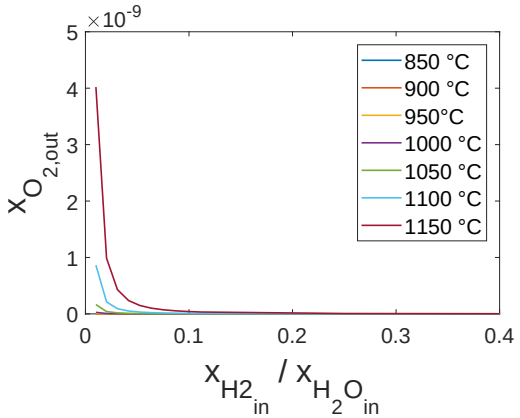

Figure C.1: Outlet molar fraction of oxygen for a system with the reactants H_2 and H_2O in different ratios.

Furthermore, the effect of introducing NH_3 to the system of H_2/H_2O is presented in Figure C.2. In similarity to when CO/CO_2 is used, very small fractions of both NO_x and N_2O are obtained. Regarding the nitrogen conversion, at 850 °C it seems like none of the introduced NH_3 is converted whereas up to 20 % of the NH_3 is converted to N_2 at low reduction potentials at 1150 °C, see Figure C.3. The resulting product is N_2.

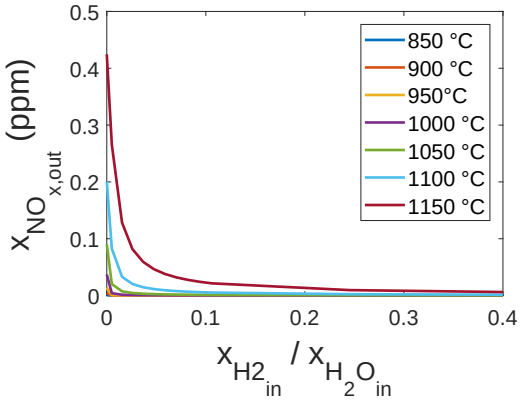

Figure C.2: Outlet molar fraction of NO_x for a system with the reactants H_2, H_2O and NH_3.

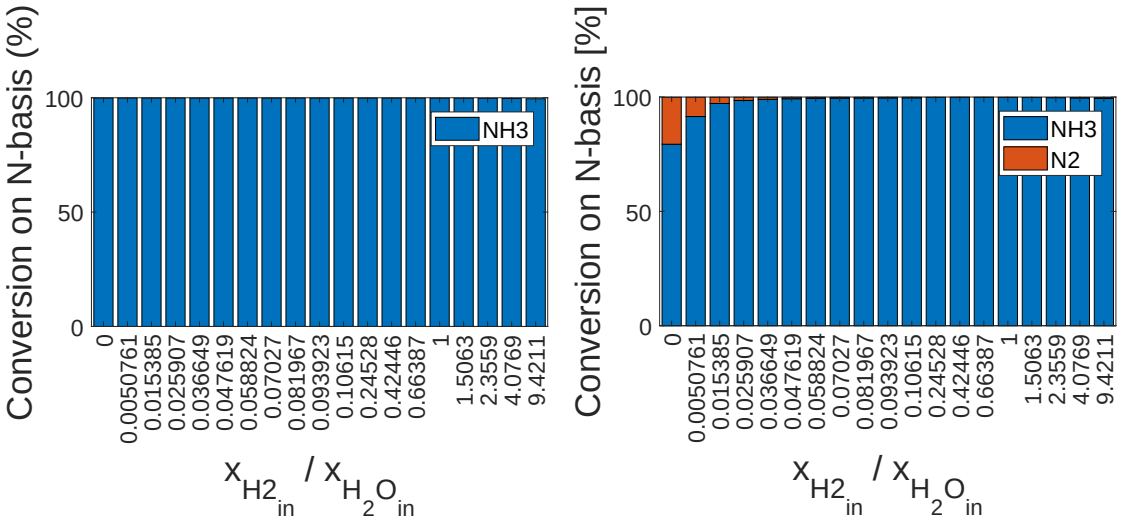

(a) **(b)**

Figure C.3: **(a)**: Nitrogen conversion for a system with the reactants H_2, H_2O and NH_3 at the temperature 850 °C. **(b)**: Nitrogen conversion for a system with the reactants H_2, H_2O and NH_3 at the temperature 1150 °C.

C.2 Me/MeO Subset in CHEMKIN

The following subset describing the heterogeneous reactions between gaseous nitrogen species and the OC is included in the extensive gas phase mechanism created by Mendiara and Glarborg [55]. The first column corresponds to the reaction, followed by k_0, β and E_a from Equation (2.30). The command FORD adjusts the order of reaction of the forward reaction.

```
! ****************************************************************************
!        MeO/Me subset                                                       *
! ****************************************************************************
```

```
!
2NH3=>N2+3H2                                  1.8828E6 0 3.5069E4!
FORD /NH3 1/                                                     !
2NH3+5MEO=>2NO+3H2O+5ME                       28.3213 0 6.4369E3!
FORD /NH3 1/                                                     !
FORD /MEO 0/                                                     !
2NO+2ME=>N2+2MEO                              6.9066E-10 0 -4.9168E4!
FORD /NO 1/                                                      !
FORD /ME 0/                                                      !
```

C.3 Reduction of Ilmenite with NH_3

In Figure C.4, the temperature dependency for when reducing ilmenite with NH_3 is presented for all concentrations.

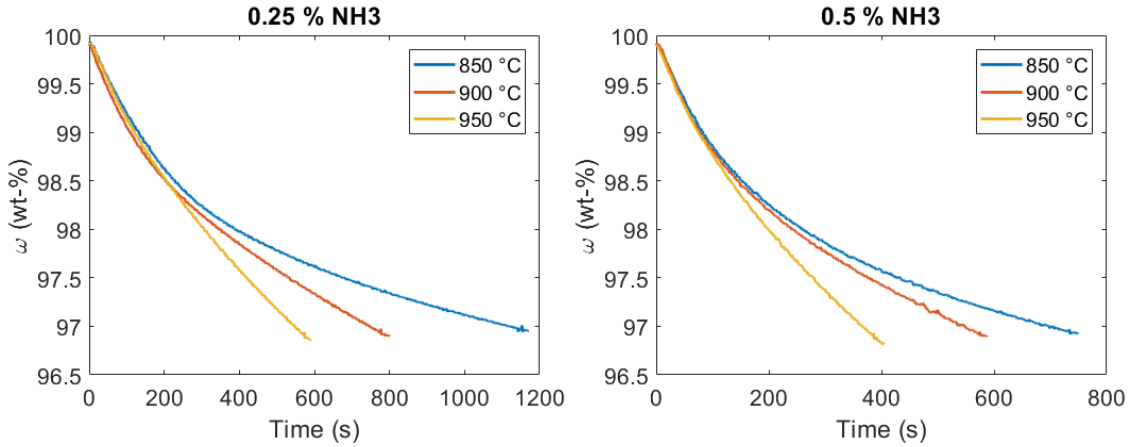

(a) **(b)**

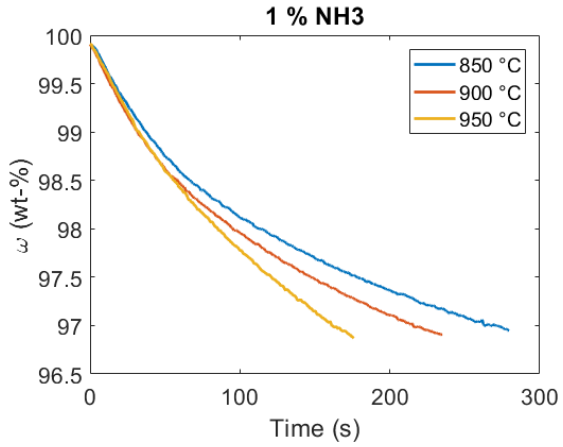

(c)

Figure C.4: The mass-based OC conversion, ω, plotted against the time during the reduction of ilmenite at 850 °C, 900 °C and 950 °C with (a) 0.25 % NH_3, (b) 0.5 % NH_3 and (c) 1 % NH_3.

The reduction of ilmenite with NH_3 at 900 °C is fitted to the shrinking core model, see section 5.2.1 for further description. In Figure C.5, the experimental values are presented alongside with the model predictions.

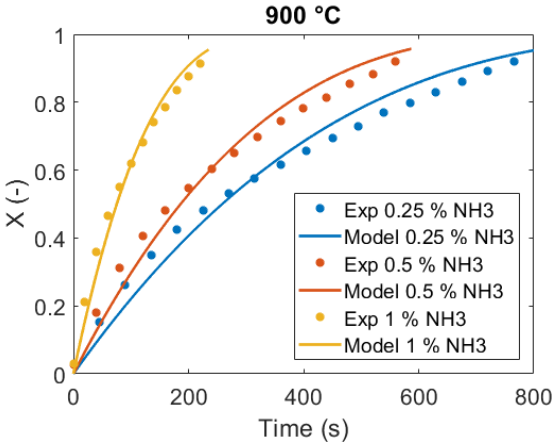

Figure C.5: Experimental values (Exp) and model predictions (Model) based on the shrinking core model of the solid conversion level, X, plotted against the time for the reduction of ilmenite with NH_3 at 900 °C.

The cyclic stability of ilmenite when being reduced with 1 % NH_3 at 850 °C is presented in Figure C.6. The second cycle is slower compared to the first cycle, whereas the reduction time increases with cycle number after that. The first cycle shows a slightly different behaviour compared to the following three cycles. It is common that the first cycle deviates from the rest when conducting TGA experiments. Furthermore, the OC can undergo both physical and chemical changes during the cycles which can affect the performance. Previous studies have shown that iron migrates towards the surface and that an iron enriched layer forms around the particle [73]. An increase in porosity has also been observed [73], together with an increase of pores inside the particle [64].

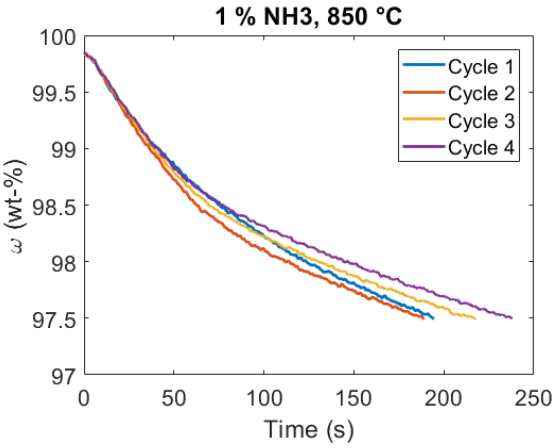

Figure C.6: The mass-based OC conversion, ω, plotted against the time during four consecutive cycles of reduction of ilmenite with 1 % NH_3 at 850 °C.

C.4 Oxidation of Ilmenite with NO

In Figure C.7, the temperature dependency for when oxidising ilmenite with NO is presented for all concentrations.

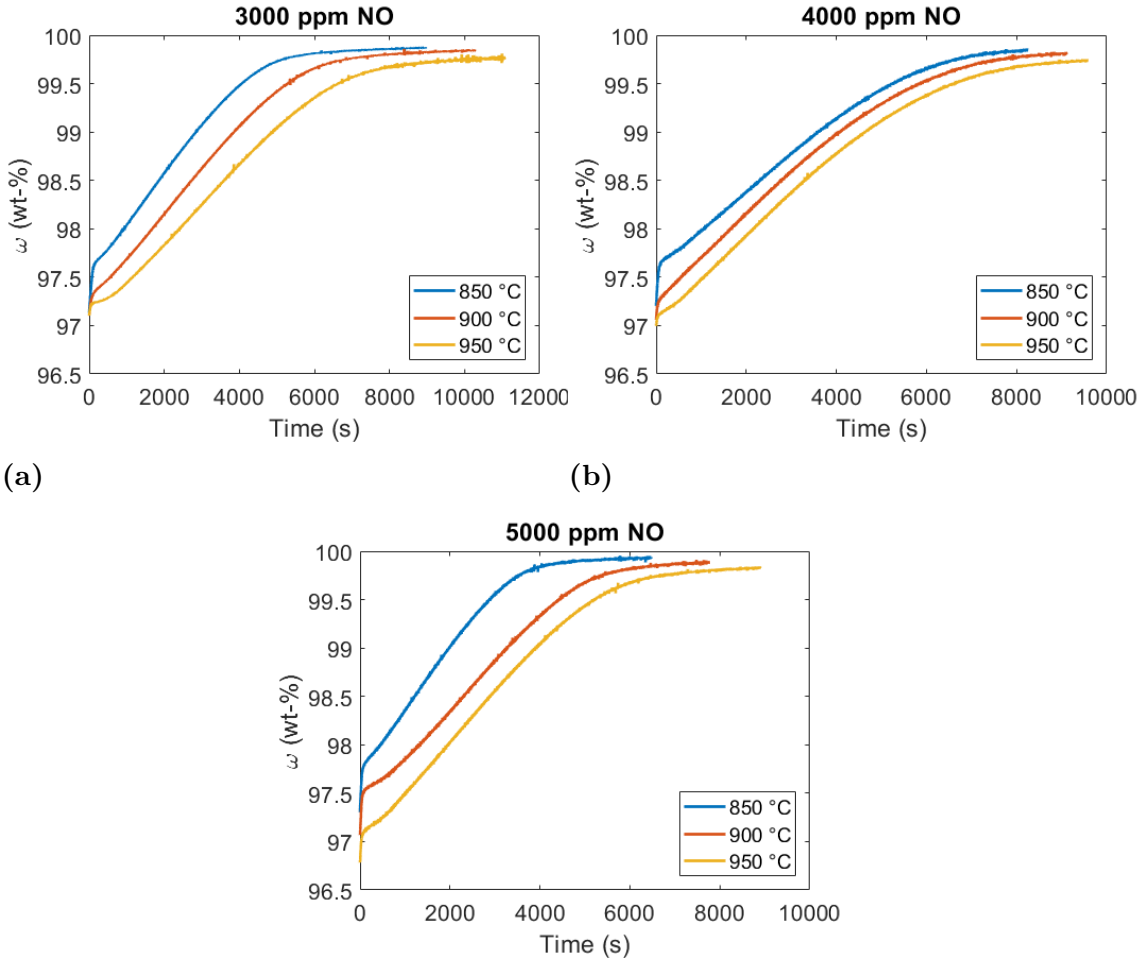

(a) (b)

(c)

Figure C.7: The mass-based OC conversion, ω, plotted against the time during the oxidation of ilmenite at 850 °C, 900 °C and 950 °C with (a) 3000 ppm NO, (b) 4000 ppm NO and (c) 5000 ppm NO.

The oxidation of ilmenite with NO is fitted to an empirical linear model, for further description, see section 5.2.2. The experimental values and the corresponding model predictions are presented in Figure C.8, C.9 and C.10.

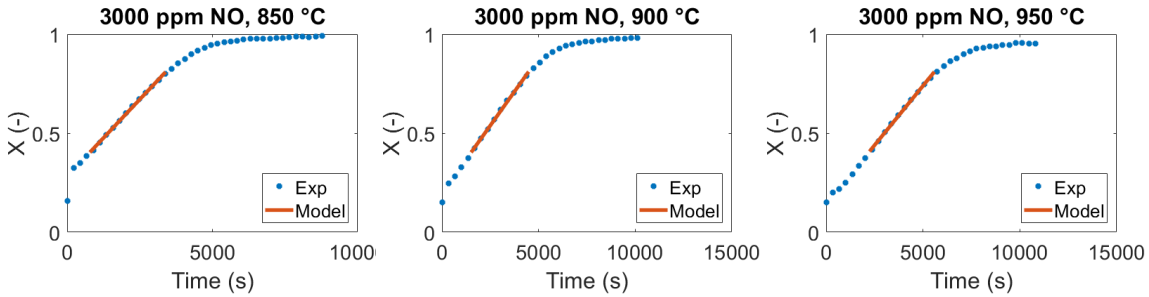

(a) **(b)** **(c)**

Figure C.8: Experimental values (Exp) and model predictions (Model) based on a linear fitting of the solid conversion level, X, plotted against the time for the oxidation of ilmenite with 3000 ppm at (a) 850 °C, (b) 900 °C and (c) 950 °C.

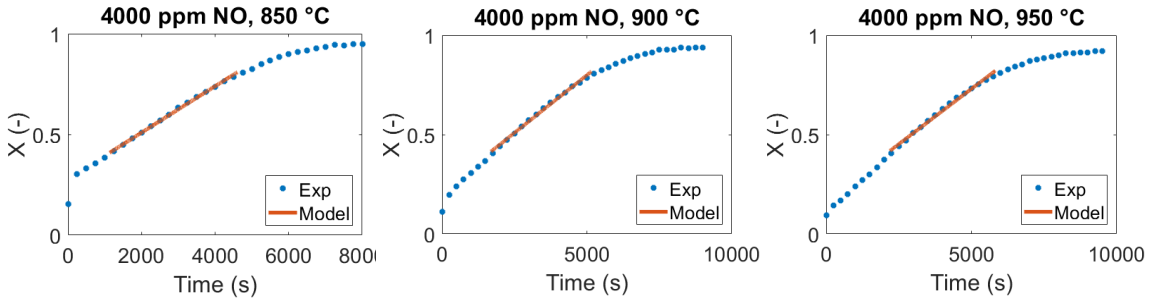

(a) **(b)** **(c)**

Figure C.9: Experimental values (Exp) and model predictions (Model) based on a linear fitting of the solid conversion level, X, plotted against the time for the oxidation of ilmenite with 4000 ppm at (a) 850 °C, (b) 900 °C and (c) 950 °C.

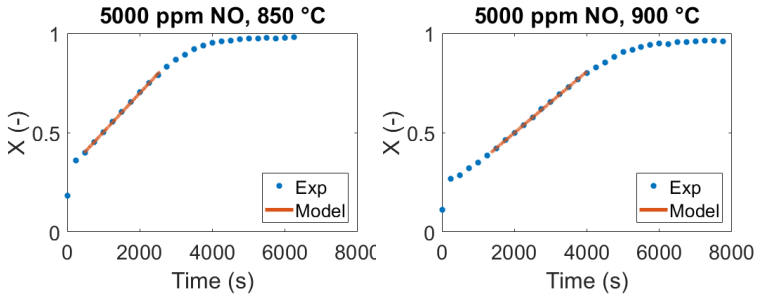

(a) **(b)**

Figure C.10: Experimental values (Exp) and model predictions (Model) based on a linear fitting of the solid conversion level, X, plotted against the time for the oxidation of ilmenite with 5000 ppm at (a) 850 °C and (b) 900 °C.

The cyclic stability of ilmenite when being oxidised with 5000 ppm NO at 850 °C is presented in Figure C.11. The first cycle deviates slightly from the following two, which are basically identical. See the section above regarding the reduction of ilmenite with NH_3 for discussion regarding cyclic stability.

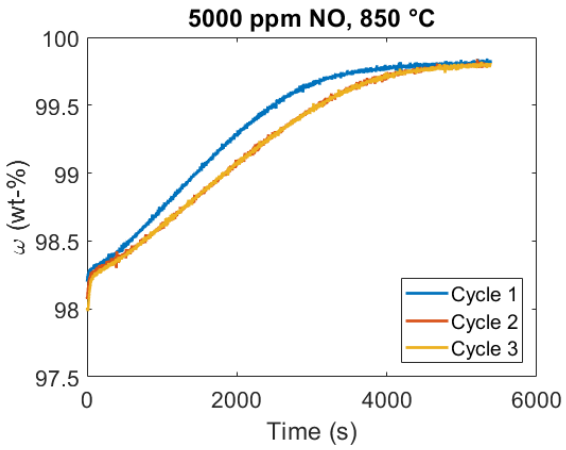

Figure C.11: The mass-based OC conversion, ω, plotted against the time during three consecutive cycles of oxidation of ilmenite with 5000 ppm NO at 850 °C.

D

Weight Gain During Inert Phase

As an action to address the observed weight increase during the inert phase, experiments where the OC is reduced with syngas followed by an inert phase are conducted, see Figure D.1. The weight gain is occurring with a constant rate until an oxidation potential corresponding to approximately 99.5 wt-% is reached, where the rate decreases. The rate is increasing with increased temperature. In Table D.1, the rates of the weight gain during inert phase are presented alongside with the rates when oxidising ilmenite with NO (during the middle part of the oxidation) as reference values.

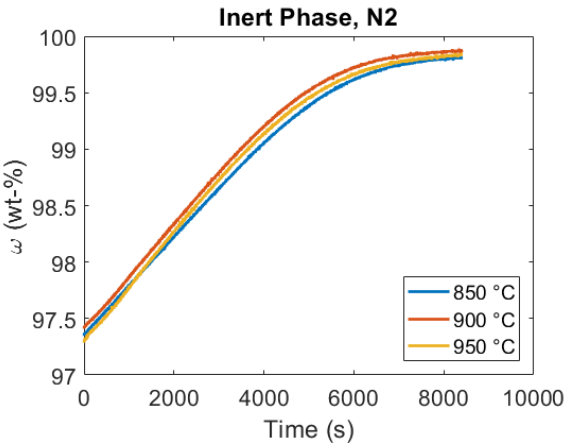

Figure D.1: The mass-based OC conversion, ω, plotted against the time during the weight gain of ilmenite during inert phase (N_2) at 850 °C. 900 °C and 950 °C.

Table D.1: The rate of which the OC gains weight during inert phase and during the oxidation with NO.

T (°C)	Rate during inert phase (wt-%/s)	Rate during NO oxidation (wt-%/s)
850	$4.2{\cdot}10^{-4}$	$1.3\text{-}2.2{\cdot}10^{-4}$
900	$4.5{\cdot}10^{-4}$	$1.4\text{-}1.6{\cdot}10^{-4}$
950	$4.6{\cdot}10^{-4}$	$1.2\text{-}1.6{\cdot}10^{-4}$

D.1 Discussion

The weight gain is rather linear with respect to the time, and if the gas is not changed, it continues until the sample reached its fully oxidised weight, where the weight gain stops, see Appendix D. Thus, it is unlikely that the weight increase is due to drift or other operational causes. That the weight stabilised at a fully oxidised level argues that an oxidation of the sample is occurring. The oxidation is assumed to be due to an oxygen leak to the system. The weight gain is, however, slow, which indicates that only small fractions of oxygen is present. Furthermore, the rate is decreased when increasing the sample mass, again arguing for small amount of oxygen. The inert phase consists of N_2, with a purity of 99.99 % at the source. Leakage in the delivery system is not likely and no leakages were detected in the TGA.

The rate during the inert phase is higher compared to the rate during exposure of NO, see Appendix D for rates. This is probably a result from either that small amounts of oxygen are present in the furnace or that it actually is NO that oxidises the ilmenite instead of oxygen. If the TGA was malfunctioning and air was leaking into the furnace, the leakage is expected to be of the same magnitude regardless of the composition of the gas flow as the same flow rates are used. Thus, smaller amounts of oxygen should not be possible during the oxidation of ilmenite with NO due to a malfunctioning TGA. That argues that the inert gas is contaminated with oxygen already before entering the TGA furnace. The results also support this hypothesis, as the reaction rate is ranked from highest to lowest for the concentrations 5000 ppm, 3000 ppm and 4000 ppm NO. For further elaboration regarding this, see Section 6.2.

E

Mass Transport

A collection of the experiments conducted with TGA has been repeated with different sample masses to investigate a possible mass transport dependency. For a purely kinetically controlled process, no difference in reaction time is expected. In Figure E.1, the distribution of the sample in the TGA crucible is shown for the four different masses investigated, ranking from increasing mass from left to right.

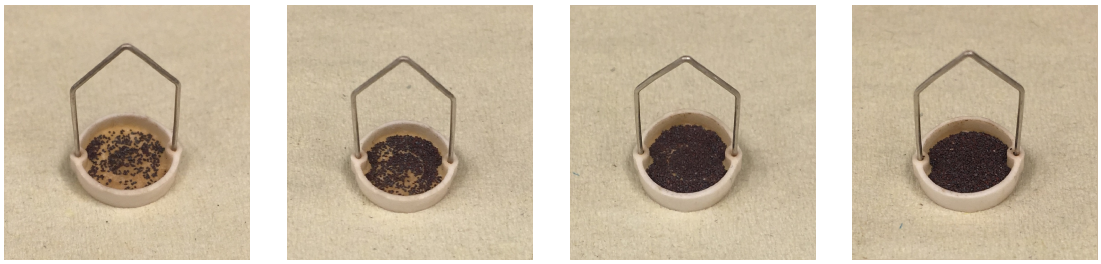

(a) **(b)** **(c)** **(d)**

Figure E.1: The crucible filled with approximately (a) 7 mg, (b) 12 mg, (c) 22 mg and (d) 42 mg of ilmenite.

To be able to discuss the experimental results, different mass transport phenomena are described in the following list:

- **Film transport:** A film will form around the particle surface due to the concentration gradient between the bulk flow and at the particle surface. The size of the film is a function of the particle diameter.

- **Interlayer transport:** If layers of particles form, the species need to transport from the outer to the inner layer and vice versa. How the particles are arranged and the total distance the species need to be transported affect the mass transport. Low amounts of layers and porously packed particles favour faster transport. With a high number of layers, the gradient over the layers, and thus the driving force, will be smaller, resulting in slower mass transport.

- **Internal transport:** If the reaction is not surface-bounded, an internal transport inside the particles will occur. The porosity and the pore structure affect the rate of which the internal mass transport occurs with. High porosity favours faster internal mass transport inside the particles.

- **Gas starvation:** When a gas flow is too small to ensure a specified bulk concentration of reactant species, gas starvation can occur as the concentration reaches zero.

Neither the film transport nor the internal mass transport should explain differences in reduction and oxidation times between different masses. Both the film transport and the internal mass transport are dependent on the particle size and structure, which are not changed throughout the experiments. However, it does not exclude the possibility of these mass transports to be of importance.

E.1 Reduction of Ilmenite with NH_3

In Figure E.2, the reduction of ilmenite with 1 % NH_3 at 850 °C and 950 °C are presented for four different masses of ilmenite. The reduction time increases with increased mass of ilmenite. Thus, mass transport seems to play an important part in the reduction of ilmenite with NH_3.

Calculations on how much NH_3 that is theoretically consumed during the reduction of ilmenite show that an NH_3 depletion of approximately 13-27 % and 34-52 % occurs at 6.9 mg and 41.7 mg respectively. The gas depletion increases with increased sample mass and increased temperature. It is not enough to cause a complete gas starvation, but it is however a substantial concentration loss. The assumption that the bulk concentration throughout the entire experiment is corresponding to the inlet concentration is therefore not appropriate. The result of the gas depletion is that the concentration is lower than the assumed, resulting in an underestimation of the kinetic parameters.

The increased reducing time when increasing the sample mass can be due to transport through the layers. The reduction times for the two smallest masses are rather similar and neither of them have enough particles to fill the crucible completely, see Figure E.1. Only small, local, layers are expected in the second smallest mass, see Figure E.1, explaining the small difference in reduction times. Regarding the temperature dependency, the reduction times have a larger distribution at higher temperatures, with the exception of the reduction times with the masses 12.4 mg and 22.2 mg. The rate of reaction increases at higher temperatures, and the mass transport is not expected to be influenced by the temperature to the same extent, resulting in that the mass transport is more likely to be the rate limiting step at higher temperatures. This is in line with the results and is therefore also arguing that a mass transport dependency exists. Furthermore, a linear dependency is expected if mass transport is rate limiting, which can be seen at the higher masses at the highest temperature investigated.

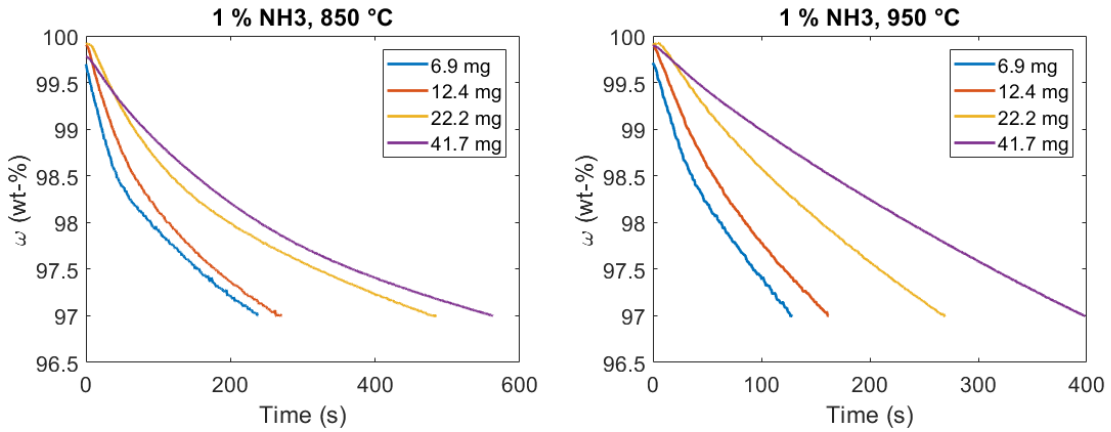

(a) **(b)**

Figure E.2: Oxidation of ilmenite with four different masses of NH_3 at (a) 850 °C and (b) 950 °C.

E.2 Oxidation of Ilmenite with NO

In Figure E.3, the oxidation of ilmenite with 5000 ppm NO at 850 °C and 950 °C is presented for two different masses of ilmenite. The oxidation times increases with increased mass of ilmenite.

Due to the long reaction times, no substantial gas depletion occurs. The remaining mass transport phenomena is the mass transport across the layers. In contrast to the results from the reduction of ilmenite with NH_3, the spread in oxidation times is smaller at higher temperature for the oxidation of ilmenite with NO. Note, however, that the rate of reaction decreases with increased temperature. When increasing the temperature, the reaction could therefore be more kinetically limiting than at lower temperatures, resulting in more similar oxidation times at higher temperature.

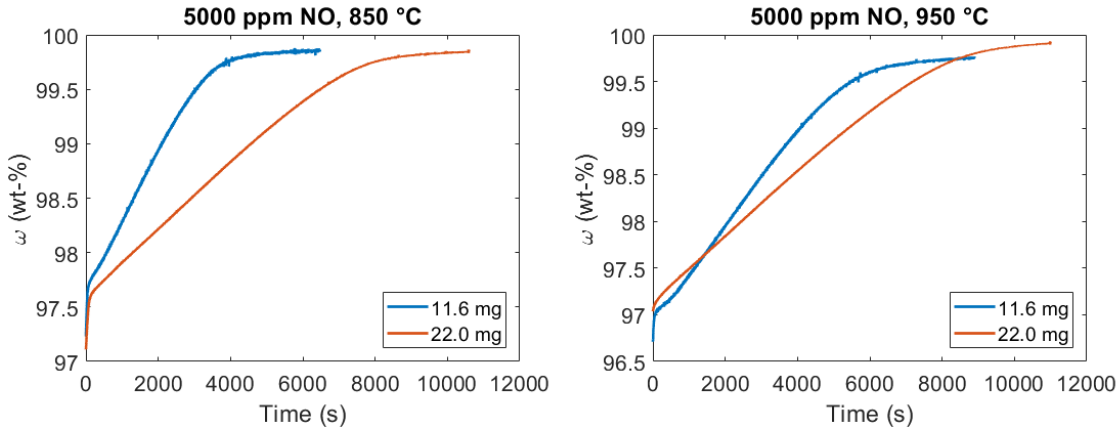

(a) **(b)**

Figure E.3: Oxidation of ilmenite with two different masses of NO at (a) 850 °C and (b) 950 °C.

E.3 Discussion

When changing the sample mass, the time to reach a 3 wt-% change is affected greatly. This argues that the reaction is not solely kinetically controlled. Regarding the experiments involving the reduction of ilmenite with NH_3, the second smallest mass investigated is used throughout the experiments and the kinetic derivation is based on that mass. A small difference in reduction times is seen at the two lowest masses investigated, arguing that the reactions are, at least partially, controlled by the kinetics at those masses. This supports the method of obtaining kinetic parameters with the used sample mass. The same extensive investigation is, however, not conducted for the oxidation of ilmenite with NO, and the same legitimacy of the method cannot be made for that case.

The effect of changing the sample mass needs to be further studied and evaluated. To obtain a purely kinetically controlled reaction, the ratio between solid particles and the gas flow rate should be altered to a level where the gas concentration is not affected by the reaction with the solid particles. However, since that might not be the case in CLC, another approach is to investigate the mass transfer rather than trying to eliminate it. To elaborate regarding what kind of mass transport phenomena that occurs, further experiments involving changing the particle size is required. It would also be of interest to compare the results when having the same mass but in different formations; one with a thin layer to avoid mass transport through the layers of particles and one with the particles clumped together to enhance the possible mass transport through layers.